

Thesis for the degree of Licentiate of Philosophy

STRUCTURE AND OXYGEN SENSITIVITY OF
ENDOEDRAL FULLERENES

MARTIN JÖNSSON



GÖTEBORG UNIVERSITY

Department of Physics

Göteborg 2005

Structure and oxygen sensitivity of endohedral fullerenes
Martin Jönsson

© Martin Jönsson, 2005

Atomic Physics
Department of Physics
Göteborg University
SE-412 96 Göteborg
Sweden

Chalmersbibliotekets reproservice
Göteborg 2005

STRUCTURE AND OXYGEN SENSITIVITY OF ENDOHEDRAL FULLERENES

Martin Jönsson
Atomic Physics
Department of Physics
Göteborg University
SE-412 96 Göteborg, Sweden

Abstract

The endohedral fullerenes Li@C_{60} and Li@C_{70} were produced using low energy ion bombardment of empty fullerenes and the material was separated and purified using High Performance Liquid Chromatography. Two fractions of Li@C_{60} and one fraction of Li@C_{70} , as determined by laser desorption time-of-flight mass spectrometry (LD-TOFMS), were studied using UV-Vis, Infrared and Raman spectroscopy, as well as electron paramagnetic resonance. It was determined that Li@C_{60} exists in the form of double-bonded dimers and closed triangle trimers.

The oxygen sensitivity of thin films of La@C_{82} was studied using LD-TOFMS. It was shown that after exposure to air the endohedral fullerene showed an increased propensity to lose the internal lanthanum atom in the laser desorption process.

Measurements of the conductivity of thin films of Li@C_{60} and La@C_{82} showed that the resistivity of the endohedral fullerenes is much lower than that of pristine C_{60} . However, the conductivity decreased dramatically upon exposure of the films to atmospheric oxygen. The effect was significantly faster for Li@C_{60} than for La@C_{82} .

Keywords: fullerenes, endohedral fullerenes, UV-Vis, IR, Raman, EPR, time-of-flight, laser desorption mass spectrometry, transport measurements.

Sammanfattning

De endohedrala fullerenerna Li@C_{60} och Li@C_{70} producerades genom att tomma fullerener bobarderades av joner med låg energi. Materialet separerades och renades med hjälp av vätskekromatografi. Det finns två fraktioner av LiC_{60} och en fraktion av Li@C_{70} , vilket fastslagits genom laserdesorptionsflykttidsmasspektrometri (LD-TOFMS), och dessa studerades med UV-Vis-, infraröd- och Raman-spektroskopi, liksom med elektronparamagnetisk resonans. Det fastställdes att Li@C_{60} existerar som en dimer med dubbelbindning mellan fullerenerna, och Li@C_{70} som en trimer i form av en sluten triangel.

Syrekänsligheten hos tunna filmer av La@C_{82} studerades med hjälp av LD-TOFMS och det visade sig att efter att ha exponerats för luft uppvisade den endohedrala fullerenes en ökad benägenhet att förlora den interna lantanatomen i laserdesorptionsprocessen.

Mätningar av konduktiviteten hos tunna filmer av LiC_{60} och La@C_{82} resulterade i en mycket lägre uppmätt resistivitet hos de endohedrala fullerenerna jämfört med tomma C_{60} . Efter att ha utsatts för syre från luften sjönk konduktiviteten dramatiskt. Luftens påverkan var mycket snabbare på Li@C_{60} än på La@C_{82} .

Appended Papers

This thesis is partly based on work reported in the following papers, referred to by Roman numerals in the text:

- I. Lassesson, A., Gromov, A., Jönsson, M., Taninaka, A., Shinohara, A. and Campbell, E. E. B., "Oxygen reactivity of La@C₈₂ investigated with laser desorption mass spectrometry", *Int. J. Mass Spectrom.*, Vol. 228, 2003, 913-920.
- II. Gromov, A., Ostrovskii, D., Lassesson, A., Jönsson, M., and Campbell, E. E. B., "Fourier Transform Infrared and Raman Spectroscopic Study of Chromatographically Isolated Li@C₆₀ and Li@C₇₀", *J. Phys. Chem. B*, Vol. 107, 2003, 11290–11301.
- III. Popok, V. N., Azarko, I. I., Gromov, A. V., Jönsson, M., Lassesson, A., and Campbell, E. E. B., "Conductance and EPR study of endohedral fullerene Li@C₆₀", *Solid State Commun.*, Vol. 133, 2005, 499–503.

These papers are printed in the Appendix.

The following scientific publications are not included in the thesis:

- Sveningsson, M., Jönsson, M., Nerushev, O. A., Rohmund, F., and Campbell, E. E. B., Blackbody Radiation from Resistively Heated Multi-Walled Carbon Nanotubes During Field Emission, *Appl. Phys. Lett.* **81**, 1095-1097, 2002.
- Nerushev, O. A., Morjan, R.-E., Ostrovskii, D. I., Sveningsson, M., Jönsson, M., Rohmund, F., and Campbell, E. E. B., The temperature dependence of Fe-catalysed growth of carbon nanotubes on silicon substrates; *Physica B* 323, 51-59, 2002.

Contents

1	Introduction	1
1.1	Filling the centre	3
2	Experimental	5
2.1	Production of endohedral fullerenes	5
2.1.1	Low energy ion implantation	6
2.1.2	A new ion source	8
2.2	Purification and characterisation using HPLC	10
2.3	Time-of-flight mass spectrometry	13
2.4	Raman and IR spectroscopy	15
2.4.1	The structure of Li@C ₆₀ and Li@C ₇₀	16
2.5	Electron paramagnetic resonance	18
2.6	Conductivity of thin films	19

3	Results and Discussion	21
3.1	Separation of Li@C ₆₀ and Li@C ₇₀	21
3.1.1	Production of Na@C ₆₀ and K@C ₆₀	25
3.2	Spectroscopy on metallofullerenes	27
3.2.1	UV-Vis spectroscopy of La@C ₈₂	27
3.2.2	Vibrational spectrum of Li@C ₆₀	30
3.2.3	Vibrational spectrum of Li@C ₇₀	33
3.2.4	Motion of the encapsulated atom	36
3.3	EPR measurements on Li@C ₆₀	38
3.4	Effect of oxygen on endohedral fullerenes	41
3.4.1	LD-TOFMS on films of La@C ₈₂ exposed to oxygen . . .	41
3.4.2	Conductivity of thin films	46
4	Conclusions and Outlook	53
	Acknowledgements	55
	Bibliography	57

1

Introduction

Born out of the fiery chasms of star cores, carbon is of one the most abundant elements in the universe. With more than six and a half million compounds of carbon known, it is arguably the most studied element of all. Not only because life as we know it would be impossible without the carbon as a building block, but, in the form of hydrocarbon polymers it bears great economic value and can maybe be said to define our plastic and petroleum age. Before long carbon might even come to replace silicon as our element of choice for electronic components (see e.g. [1]).

From ancient times until recently pure carbon was thought to exist in only two different allotropes — diamond and graphite. In its most dazzling form, the diamond, each carbon atom binds to four neighbouring atoms with covalent σ -bonds in a tetrahedral structure. In essence, each diamond can be considered a single molecule, and the result is a material with exceptional properties: It is the hardest of all known substances, although brittle, it has the highest thermal conductance, a very high melting point, and a high refractive index. The latter gives the diamond its enticing brilliance. In graphite each carbon atom binds to three other atoms forming a vast sheet of hexagonal rings (graphene sheets). The bonds within the sheets are stronger than those in diamond, but the weak van der Waals bond between sheets stacked on top of each other gives graphite a quasi-two-dimensional layered structure. Delocalised π -bonds in the graphene sheet makes graphite electrically conducting along the layers, but insulating perpendicular to them.

In 1984 Rohlffing, Cox, and Kaldor, working for Exxon, used a laser to vaporise a graphite disc under a flow of high pressure helium, creating a supersonic carbon cluster beam. A strange pattern of even-numbered carbon clusters with 40 to over 100 atoms were found [2]. Rohlffing *et al.* attributed the new clusters to a hypothetical form of carbon called carbyne which would consist of a chain with alternating single and triple bonds. A year later H. W. Kroto, R. F. Curl, and R. E. Smalley, with the students J. R. Heath and S. C. O'Brien, using a similar setup to study the properties of long carbon chains known to exist in interstellar space, found the same clusters. By fine-tuning their equipment they found that some species, especially C_{60} , were particularly stable. Kroto *et al.* correctly deduced that C_{60} has the structure of a normal football, a truncated icosahedron. [3]

The truncated icosahedron has 32 faces, 12 pentagons and 20 hexagons. The geometrical shape was known already by the Ancient Greeks, and it was depicted by Leonardo da Vinci. Euler showed that closed cage structures of this kind can be built by any number of hexagons (except 1) and always 12 pentagons. The number of vertices, or atoms, is always even. The American architect and inventor R. Buckminster Fuller had been constructing spherical buildings called geodesic domes (see fig. 1.1), most famously at the Expo'67 in Montreal, of a similar structure. In his honour the new molecule, C_{60} , was named *Buckminsterfullerene*, or fullerene for short.

Even though the proposed structure was controversial during the first years, evidence amassed from e.g. NMR to confirm the assumption, and in 1996 the discovery of the fullerenes was awarded with the Nobel prize in chemistry to Kroto, Curl, and Smalley. [4] A decisive contribution to the field of fullerene research was made in 1990 by Krätschmer and co-workers when they, using arc-discharge vaporisation of a graphite rod, succeeded in producing macroscopic amounts of C_{60} that enabled an array of experiments to be performed. [5] Today fullerenes attract the attention of scientists from many different disciplines of physics and chemistry, but also in biology and medicine. Many fullerene species are available commercially and a number of new applications based on fullerenes have been proposed. For this to be realised diverse properties of fullerenes have been studied, in the gas phase, in solid form, at different temperatures and using almost all tools in the physics toolbox, see e.g. [6]. Due to its high symmetry, it belongs to the most symmetrical I_h point group, C_{60} has, in the spirit of Thoreau to simplify [7], become a favourite model system for many kinds of cluster experiments. [8,9]

From the discovery of C_{60} , the mass spectrometer has been one of the most important instruments for fullerene studies, and it has been used extensively for the work in this thesis.

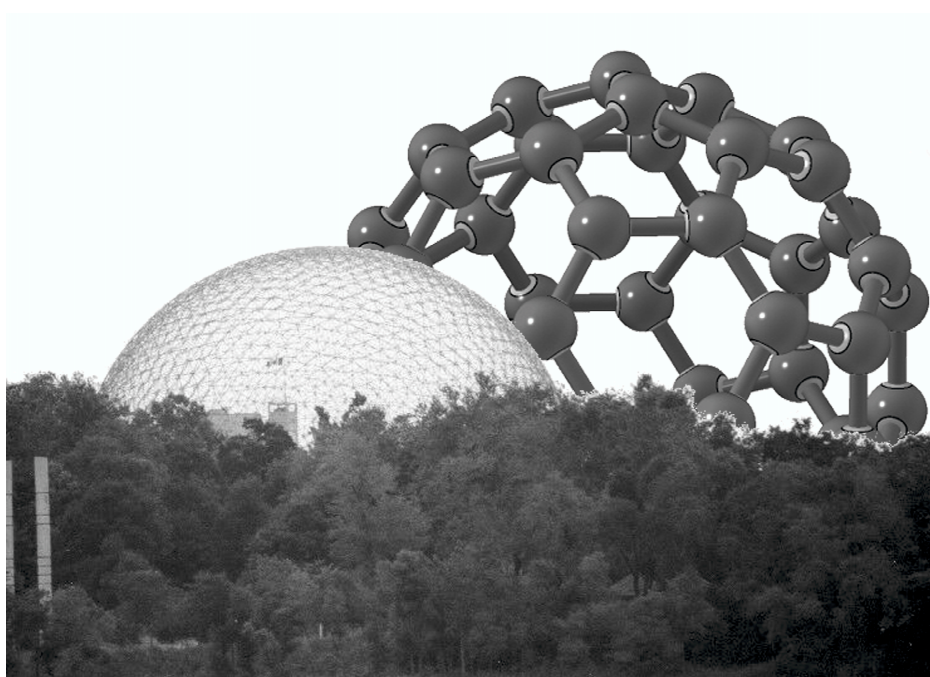


Figure 1.1: The American pavilion at the Expo '67 in Montreal, designed by R. Buckminster Fuller. Superimposed is a model of the fullerene C_{60} .

1.1 Filling the centre

As the fullerenes consist of a hollow cage of carbon atoms it was realised, almost immediately after their discovery, that different atoms or molecules could be introduced into the centre [10]. These molecules, with incorporated atoms, became known as *endohedral fullerenes*, from Greek $\epsilon\nu\tau\acute{o}\varsigma$ meaning within and $-\epsilon\delta\rho\omicron\nu$ meaning base or seat. The standard notation for indicating that an atom is trapped within the carbon cage is $X@C_n$, where X is the confined particle.

The incorporation of atoms in the fullerene interior would scarcely be interesting if it did not affect the molecule as a whole. The presence of the guest atom does change the behaviour of the fullerene in many ways; by donating charges to the carbon cage the molecule's electronic properties can be significantly altered, changing it from semiconducting to metallic, the position of the atom inside the shell can modify the molecular symmetry, opening up previously silent vibrational modes, that can be measured using Raman and Infrared spectroscopy. Furthermore, the carbon cage will protect the enclosed atom from the environment, making it less volatile. This has led to experiments using endohedral fullerene

derivatives, especially with encapsulated gadolinium, as MRI contrast agents that might rival current commercial Gd agents [11, 12].

The most available and therefore most investigated endohedral fullerenes are rare-earth containing C_{82} . These are readily soluble in standard solvents like carbon disulfide (CS_2), and can be purified using liquid chromatography. The metal-containing C_{60} have proven difficult to purify, but nevertheless our group has developed a method for production and purification of $Li@C_{60}$. An authoritative review on endohedral fullerenes was recently written by Hisanori Shinohara [13]. Recently it was also reported that the enclosure of 7Be in a C_{60} influences its radioactive half-life [14].

This thesis will dilate upon the production of, and experiments on, $Li@C_{60}$. It will also discuss some results concerning $La@C_{82}$ which was produced by the Shinohara group.

2

Experimental

In this chapter the different experimental methods used for producing and analysing the endohedral fullerenes will be described. First will be a discourse about the low energy ion implantation method used in our group to produce alkali containing fullerenes. Purification of fullerenes is generally performed using liquid chromatographical methods, and this will be the topic of section 2.2. As mentioned earlier mass spectrometry is a crucial analytical method in most fullerene research, and section 2.3 will introduce the time-of-flight mass spectrometer and our measurements.

Experiments on films of endohedral fullerenes were performed to investigate the vibrational modes of the fullerenes using Raman and FTIR spectroscopy, as well as measurements of electrical properties and the influence of air on the film. Also EPR measurements have been made together with collaborators in Belarus.

2.1 Production of endohedral fullerenes

The first endohedral fullerenes were produced the same way as the first fullerenes, but using a metal doped target for the laser vaporisation. Mass spectrometry of the cluster beam showed that metal atoms were captured in the carbon cage [10]. Similarly the metallofullerenes can be produced using arc-discharge vaporisation

of a metal containing graphite rod. These methods produce a large number of both empty and filled fullerenes, and even though mass spectrometry of the soot shows that $M@C_{60}$ is often the most abundant species it has generally not been possible to extract and purify it. Of the metal containing molecules only the higher fullerenes, and in particular the $M@C_{82}$, are soluble in standard solvents like toluene or CS_2 [15, 16].

To produce endohedral fullerenes with a certain cage number one can start with empty fullerenes and try to insert atoms into them, either by shooting them through hexagon or pentagon rings in the carbon cage, or by breaking a C-C bond to open the cage [17–19]. Many methods can be used to accomplish this. Fullerenes heated to high temperature in a high pressure (ca 2500 atm) rare gas atmosphere form a tiny amount of endohedrals when some rare gas atoms manage to penetrate the carbon cage [20]. They can also be formed by introducing fullerenes into a plasma of alkali or other metals and landing them on a biased substrate [21, 22]. Neeb *et al.* succeeded in mass selecting endohedrals, created by the laser evaporation method, and depositing them *in situ* on a substrate, however in minuscule amounts [23, 24]. In our group we produce endohedral fullerenes in a process based on bombardment with alkali ions, which will be detailed below.

2.1.1 Low energy ion implantation

The production method employed in our laboratory is similar to the early gas phase collision experiments [25, 26], in which alkali and other ions were collided with neutral fullerenes. Wan *et al.* [25] showed that there was an energy threshold for insertion of Li^+ , Na^+ , and K^+ into C_{60} amounting to ~ 6 eV, ~ 18 eV, and ~ 40 eV respectively. In the case of lithium, due to its small ionic radius (~ 0.7 Å), the ion can be slipped through a hexagon in the fullerene cage whereas the larger alkalis need to break a carbon-carbon bond to open up the cage to be able to enter. Hence the higher energy thresholds for Na^+ and K^+ .

The method is fairly simple and has, in its earliest form, been described previously [27]. The whole setup, sketched in figure 2.1, is enclosed in a vacuum chamber that can be pumped down to 10^{-6} mbar. Commercially available fullerene powder, of 99.5% purity for C_{60} and 98% for C_{70} , is put in a quartz crucible that is inserted into a stainless steel oven. When the oven is heated to approximately 500 °C the fullerenes are evaporated onto a target consisting of an aluminium foil wrapped around a rotating cylinder. The rate of deposition is measured with a crystal oscillator thickness monitor, and the rotation speed of the cylinder is adjusted so that for each turn of the cylinder one monolayer of C_{60} is deposited on

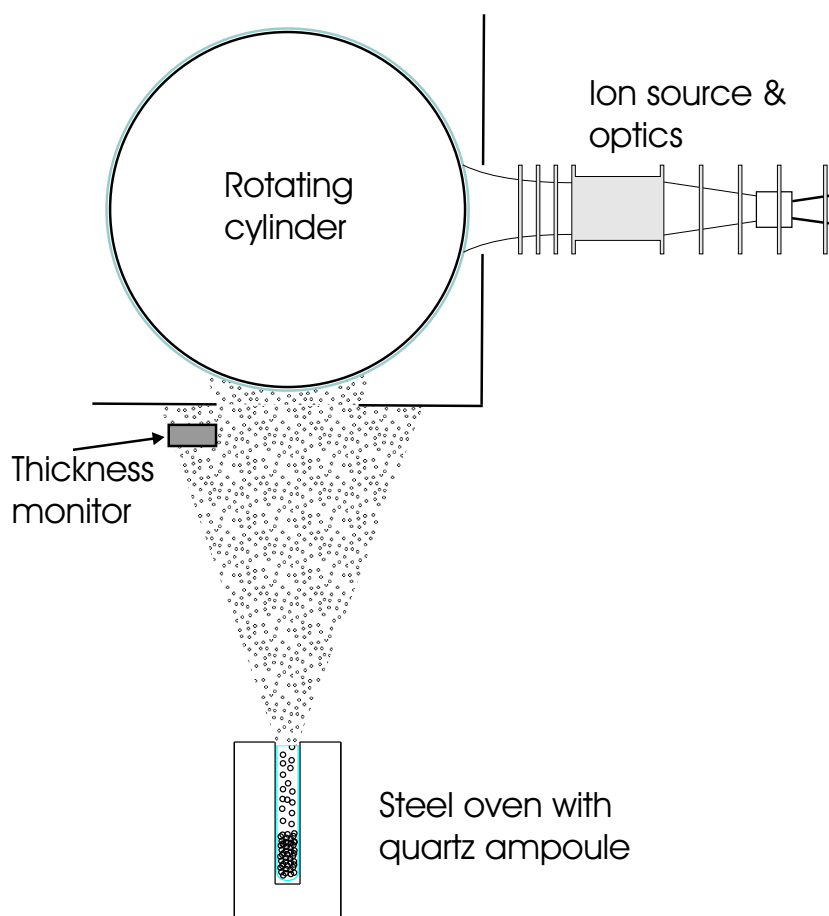


Figure 2.1: Sketch of the endohedral production setup. As described in the text the fullerenes are deposited on the cylinder and subsequently bombarded with alkali ions.

the film. Orthogonal to the C_{60} beam, a low-energy ion beam hits the cylinder. As the cylinder turns, the freshly deposited fullerene layer passes through the ion beam. This way it is ensured that every fullerene layer is irradiated with the correct ion dose. The ions come from a highly porous tungsten plug containing an alkali salt which is heated by a ceramic heater [28] (available commercially from HeatWave Labs). Operating at a temperature above $1000\text{ }^{\circ}\text{C}$, a large portion of the alkalis vaporised from the emitter is ionised by surface ionisation. The ion source is floated on a potential equal to the desired kinetic energy of the ions. Typically we use 30 V for Li, 70 V for Na and 80 V for K [29]. The energy spread of the ion beam is less than 0.5 eV . The beam can be focused or defocused by an Einzel lens to cover an area on the cylinder approximately 2.5 cm in diameter, that is covered

with fullerenes.

The ion current is strongly dependent on the temperature and can reach a few tens of μA . The current is monitored by an Amperemeter connected to the cylinder, which is isolated from the rest of the chamber. To increase the life-time of the ion emitter and decrease the radiative heating of the fullerene film and the rest of the vacuum system the ion current is limited to a few μA . In a typical experiment a fullerene deposition rate of ca $0.5 \text{ \AA}/\text{min}$ and an ion current about $5 \mu\text{A}$, is used. This corresponds to roughly 1 ion per fullerene deposited on the irradiated area. A higher ion to fullerene ratio gives a larger proportion of endohedral fullerenes as observed by mass spectrometry, but also a much larger insoluble part. [30]

2.1.2 A new ion source

The ion emitters described in the previous section are very well suited for our kind of implantation experiments. An important aspect is that the thermal ion energy distribution from the emitters lack the tail of higher energy ions that come from many other types of ion sources. However, the emitters are rather expensive, and the ions available are limited to alkali metals. Therefore we have been looking for an alternative solution to create the ions for implantation. It was tried using a modified version of a commercial ion-source, designed for Cs-ions, but the high temperatures needed to produce lighter alkali ions created problems making the source impractical to use [31].

Surface ionisation of atoms mainly takes place when an atom of low ionisation potential hits a surface with high work function. In the alkali group the lighter metals have a higher ionisation potential than the heavier, ranging from $\phi = 3.9 \text{ eV}$ for Cs to $\phi = 5.4 \text{ eV}$ for Li. The ionisation probability can be estimated with the Saha-Langmuir equation [32]:

$$P = \frac{1}{1 + \frac{\omega_+}{\omega_0} \exp\left(\frac{\phi - \Phi}{k_B T}\right)} \quad (2.1)$$

Φ is the work function of the ionising surface and T is the temperature of the surface. ω_0 and ω_+ are statistical weights equal to the degeneracy of the ground state of the neutral atom and the ion respectively. The degeneracy is given by $\omega = 2J + 1$, where J is the total angular momentum of the atom/ion.

A surface ionisation ion source that could be used for generating a lithium ion beam was constructed by Rasser and Remy [33] and modified to also be able to

ionise other element such as lanthanum [34]. The ioniser is a mesh of Rhenium, which has a work function $\Phi = 4.96 \text{ eV}$ and can sustain heating to high temperatures. A similar setup was constructed in our lab based on this prototype. The

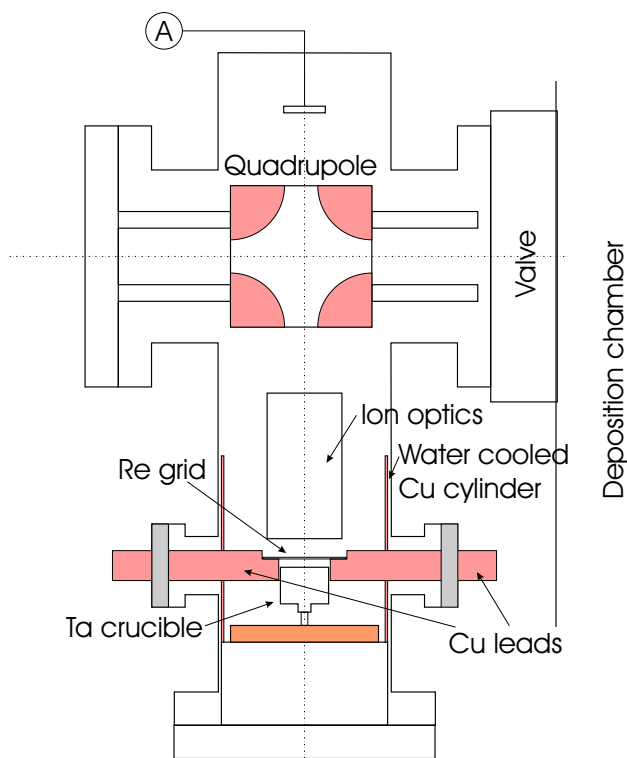


Figure 2.2: A sketch of the ion source build for generating lithium and possibly also aluminium and other ions. In the quadrupole the ions are deflected to the right where the cylinder in figure 2.1 is located.

setup can be seen in the sketch in figure 2.2. It consists of a tantalum crucible that can be heated to ca 1000°C by a heating wire wound around it, and a rhenium ioniser. The ioniser is made from a 1 mm thick Re sheet with laser drilled holes. The ioniser is heated ohmically by a high current. The ioniser can be heated to more than 1000°C , probably as high as $1800\text{--}2000^\circ\text{C}$. The crucible is placed on a thin ceramic holder on a water-cooled Cu base, and the walls of the vacuum chamber that houses the source are shielded from the heat by a water-cooled Cu cylinder. In spite of these precautions the intense heat from the ioniser has led to several difficulties¹, and the outer walls of the vacuum chamber reaches over 100°C during longer tests.

¹...including the melting of the 16 mm thick copper leads supporting the grid

Using the expression in eq. 2.1 one can calculate the ionisation probability for different atoms hitting a heated rhenium surface. The result can be seen in figure 2.3. Since the work function of rhenium is higher than the ionisation potential for potassium the probability for creating K^+ ions is very high. At a working temperature of ca 1100 °C about one third of all lithium atoms hitting the surface will ionise, while less than one in 10000 aluminium atoms will. The total ion current will of course depend also on the temperature of the crucible, that determines the flow of neutral atoms. The flow can be estimated as

$$F = \frac{\rho A v_{\text{mean}}}{2}, \quad (2.2)$$

where ρ is the density of atoms and can be estimated from the ideal gas law as $\rho = p_{\text{vap}}/k_B T_{\text{res}}$, with T_{res} the temperature of the crucible, and p_{vap} the vapour pressure at this temperature. v_{mean} is the mean velocity of the atoms and is given by

$$v_{\text{mean}} = \sqrt{\frac{8k_B T_{\text{res}}}{\pi m}}. \quad (2.3)$$

The ion current is given by

$$I = P \cdot F, \quad (2.4)$$

with P from eq. 2.1. The calculations assume, unrealistically, that all neutral atoms from the crucible hit the Re grid, and that all created ions can be extracted into the beam. However, even if the absolute numbers given by the calculations are overstated, they give an indication of which temperatures are necessary to reach some current.

2.2 Purification and characterisation using HPLC

The method of using HPLC, high pressure (or performance) liquid chromatography, for purification of metallofullerenes has been thoroughly described in the review by Shinohara [13], and this section will just give a brief sketch of the procedure used in our lab as shown in figure 2.5.

When the irradiated fullerene film has reached its desired thickness the process is stopped and the aluminium foil is removed from the cylinder and placed in a bottle under nitrogen gas. The bottle is then filled with CS_2 and placed in an ultrasonic bath for several minutes to dissolve the fullerenes. The soluble material is separated from the insoluble, consisting mostly of polymerised fullerenes and alkali salts, by filtration through a teflon filter with 0.2 μm pore diameter. The solution is

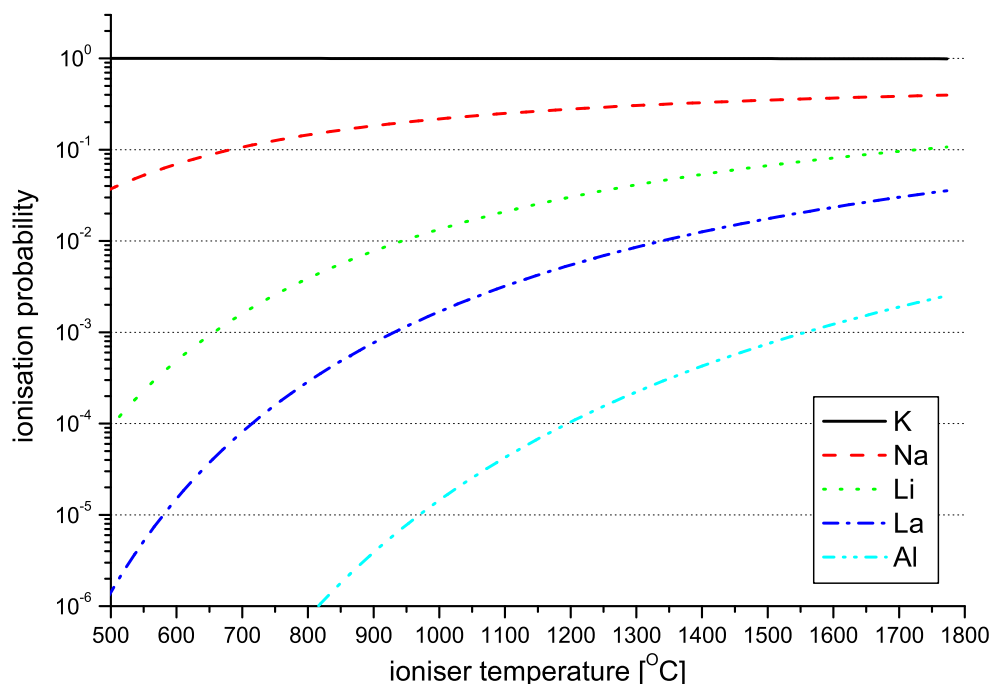


Figure 2.3: The ionisation probability of an atom hitting a rhenium surface, calculated using eq. 2.1.

dried from CS_2 in a rotation evaporator and redissolved in *ortho*-dichlorobenzene (DCB), which is used as eluent in the HPLC. In the HPLC, the solution is pushed at high pressure (~ 10 MPa) through a column (Cosmosil, 5PBB) packed with porous silica gel and a stationary phase of pentabromobenzyl. The interaction between the fullerenes and the stationary phase makes different fullerene species exit the column after different *retention times*. Past the column, the solution proceeds through a flow cell with a UV-Vis spectrometer that measures the absorption in the range 290–800 nm. At 340 nm, a wavelength strongly absorbed by most fullerene species, the abundance of fullerene material as a function of retention time is monitored, see figure 3.3. After the spectrometer, the solution passes through a valve that collects the different fractions in separate bottles according to fixed time windows.

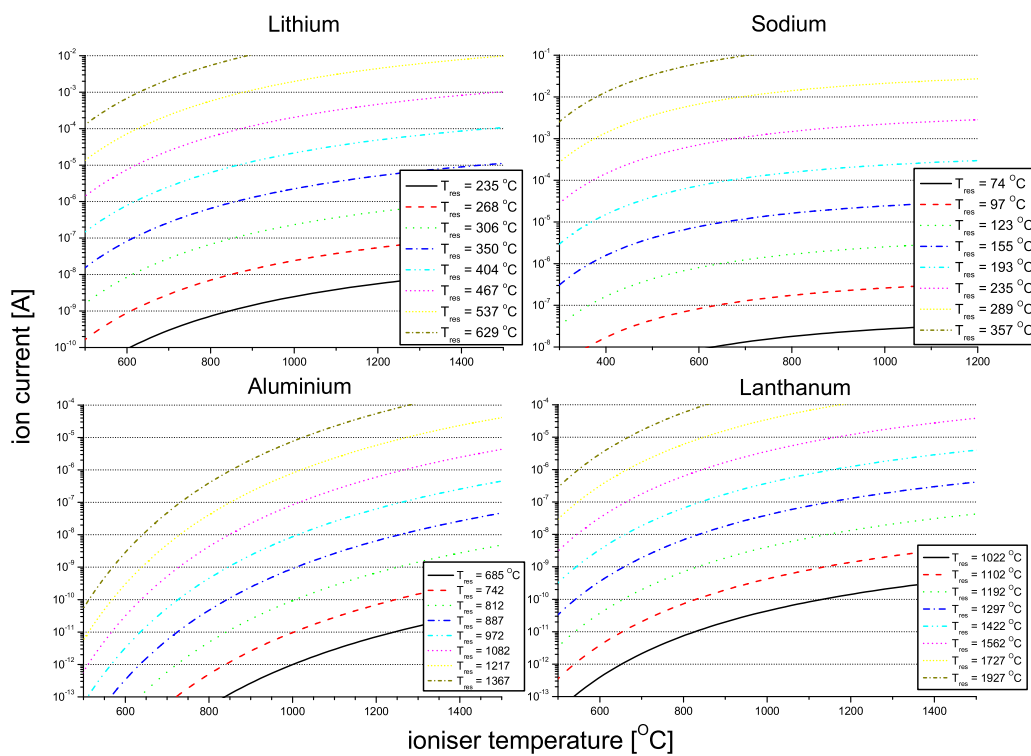


Figure 2.4: Calculated ion currents for some relevant elements using equation 2.4. Note the very high temperatures needed on both crucible and ioniser for La and Al.

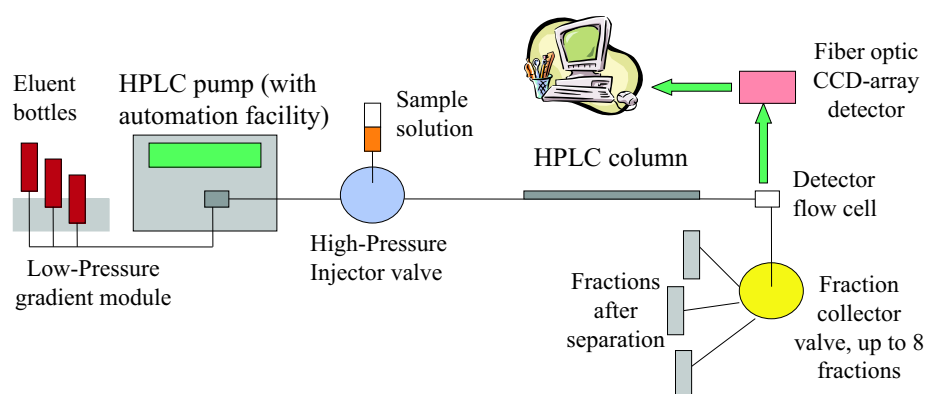


Figure 2.5: A sketch of the HPLC setup used to separate endohedral fullerenes from the empty molecules.

2.3 Time-of-flight mass spectrometry

In the field of cluster science different forms of mass spectrometry play an important role. One of the most versatile forms of mass spectrometry is time-of-flight (TOFMS), where ions are accelerated by an electric field and fly through a vacuum tube ($\sim 10^{-7}$ mbar) towards a detector. The kinetic energy of the ions will be $E_{\text{kin}} = q \cdot U = \frac{mv^2}{2}$, where q is the charge of the ion and U the accelerating potential. After the accelerating field the ions will pass through a field-free region and since all ions with the same charge have the same energy, lighter species will have a higher velocity and travel the field-free region to the detector faster than the heavier ions. In its basic form, the TOFMS has a very simple design, but still offers a high resolution, with $m/\Delta m > 1000$, and possibility to measure up to several thousand mass units. Another advantage is that in the TOF the whole mass range can be monitored in every ion pulse.

In our setup the ions are detected using a Microsphere Plate (MSP) detector [35] from El-Mul, or two Multi Channel Plates (MCP) mounted back-to-back in a so called chevron setup. For detection of positive ions, the detector is floated on a large negative potential of up to -2 kV. A voltage of 3.3 kV (2 kV for the MCP) is applied over the detector so that the front of the detector has a potential of up to -5.3 kV. Two cm in front of the detector is a grounded net that separates the field-free region from the post-acceleration region. The electrons that are released when the ions slam into the detector plate are accelerated towards a grounded anode that is connected to an oscilloscope. By reversing the polarity of the fields the spectrometer can also be used for detection of negatively charged ions.

The number of electrons from an MCP or MSP detector is known to scale with the velocity of the detected ion, rather than its energy [36, 37]. This gives a higher signal for the lower mass peaks in our spectra, something that can be problematic, especially due to the usually high amount of K^+ present in most spectra.

How the ions are created from the sample differs between various types of TOF spectrometers. In our setup we generally use laser desorption/ionisation (LD-TOFMS) to investigate the produced fullerene films. The sample is placed on the end-electrode of the spectrometer (see figure 2.6a) and a 337 nm N_2 -laser, with a pulse length of 10 ns, is used for ablating material from the surface into the gas phase. The laser is focused onto the sample by a lens with 500 mm focal length, and by moving the mirror along the beam axis the size of the laser spot on the sample, and hence the laser fluence, can be adjusted. The temperature in the plume of ejected material reaches several thousand degrees [38], and a plasma of both positively and negatively charged ions is formed. By pulsing the potential on the

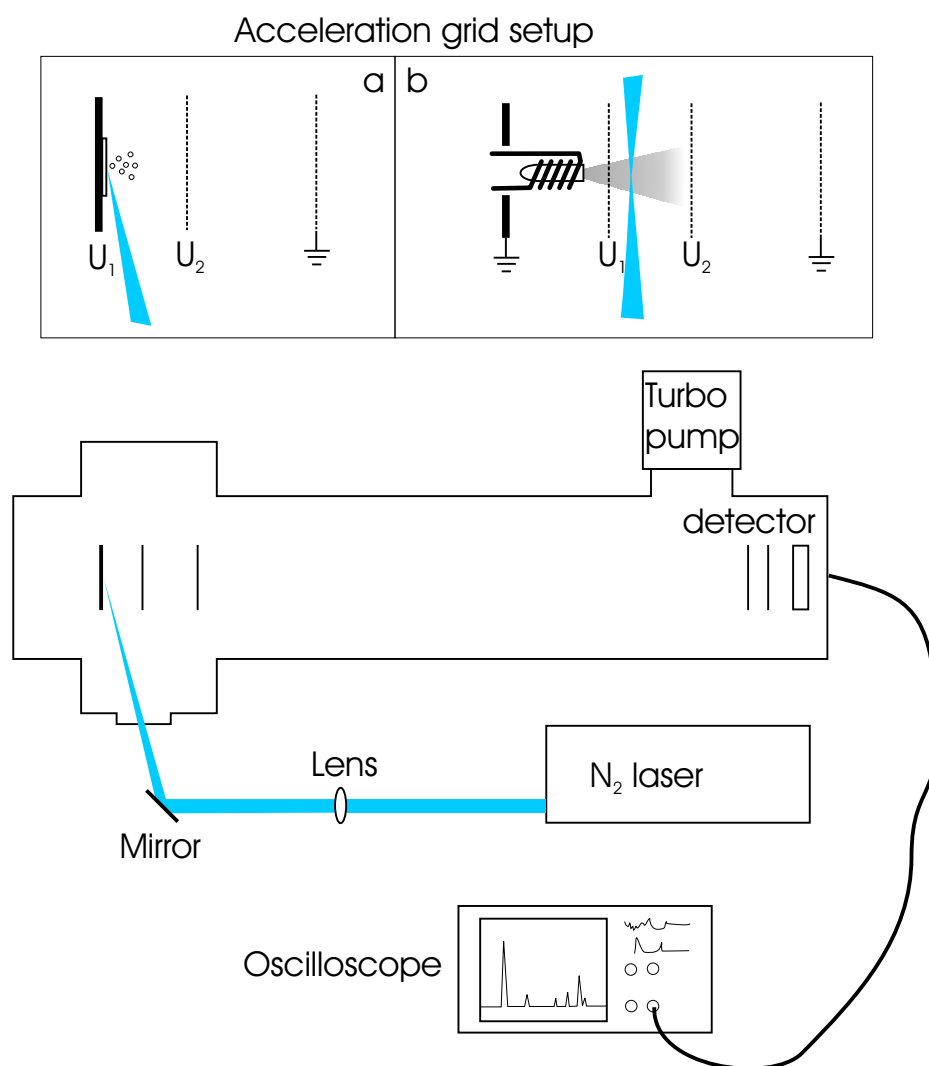


Figure 2.6: A schematic picture of the time-of-flight mass spectrometer setup and the configurations of the accelerating field electrodes when used in a) laser desorption mass spectrometry and b) gas phase mode.

electrodes the ions are accelerated. By applying different waiting times between the laser pulse and turning on the field one can learn a lot about e.g. different cooling processes of molecules. In some experiments the sample is put into a quartz ampoule that is heated by an electric heater. In this case the laser is used to ionise the material evaporated from the ampoule, see figure 2.6b.

The two accelerating fields defined by the potentials U_1 and U_2 in figure 2.6 are set up according to Wiley and McLaren [39] to provide better space focusing, that is improving the resolution by making sure that ions of the same mass located at different points in the accelerating field when the voltage is switched on reach the detector at the same time. Given a certain length of the field-free region and the distance between the electrodes, the focusing condition is given by the ratio, U_2/U_1 , of the applied voltages. The ions in our experiments will be spread out in space depending on the distribution of kinetic energy received in the laser desorption process and the time before the field is switched on. C_{60} in a laser desorption plume has been measured to have initial velocities of up to 1000 m/s [40] or about 1 mm/ μ s. Since the field is typically switched on after roughly 1 μ s the ions are still reasonably tightly gathered. So, in most of our experiments the ions are confined to a small enough region, and the TOFMS is used in a one field configuration with $U_2 = 0$.

2.4 Raman and infrared spectroscopic investigation of $Li@C_{60}$ and $Li@C_{70}$

In Raman and infrared (IR) spectroscopy the coupling of radiation to the vibrational modes of molecules or solids is used to extract information about the structure of the sample. In a molecule with N atoms there are $3N - 6$ vibrational modes (in linear molecules they are $3N - 5$) that comprise its vibrational spectrum. The specific features of the spectra depend on the geometrical arrangement of the atoms, the strength of the chemical bonds and the masses of the atoms. All in all this creates a sort of a “fingerprint” of a molecule.

Absorption of infrared light and Raman scattering are the two most important methods of examining the vibrational spectra. Not all $3N - 6$ vibrations are IR or Raman active. Only those vibrations that change the molecular dipole moment are visible in the IR spectra, and only those that modulate the polarisability are Raman active. The rest of the modes are inactive or *silent*. Due to molecular symmetries many vibrations have the same frequency, and even in a large molecule only a few peaks may be seen in the Raman and IR spectra; for example C_{60} has only ten

Raman active and four IR active modes. By comparing the strengths and positions of these peaks with known species and with calculations much information can be extracted about the structure of the sample molecule.

For our IR and Raman measurements of endohedral fullerenes, described in detail in Paper II, several samples were prepared and droplet coated on KBr discs. Samples of pure C_{60} and C_{70} were used as reference together with a sample of $(C_{60})_2$, the [2+2] dimer of C_{60} . The $(C_{60})_2$ was prepared by ball milling C_{60} in the presence of metallic lithium, according to Lebedkin *et al.* [41] Care was taken that no lithiated species ($Li:C_{60}$ or $Li@C_{60}$) were present in the purified $(C_{60})_2$. This was controlled by laser desorption mass spectrometry, which showed no presence of any peak at 727 mass units. Samples of the endohedral C_{60} were prepared from both the E1 and E2 fractions of the HPLC purified production material (see section 3.1). To enable the distinction between vibrations in the C_{60} cage and those caused by the interaction of Li with the fullerene endohedral samples were prepared using both the 6Li and the 7Li isotopes.

The IR absorption measurements were performed on a Bruker 22 Fourier transform infrared spectrometer. The setup was placed inside a glovebox with dry argon atmosphere. The spectra were taken at room temperature. The Raman scattering experiments on the other hand were done in ambient atmosphere with a Bruker IFS-66 spectrometer equipped with a Raman module and a liquid-nitrogen-cooled Ge-detector. The samples were illuminated by a 1064 nm Nd:YAG laser and the scattered light was collected in a backscattering geometry over the course of 9–16 hours per spectra. The laser intensity at the focal point was $\sim 100 \text{ W/cm}^{-2}$.

2.4.1 The structure of $Li@C_{60}$ and $Li@C_{70}$

The fullerene C_{60} has 174 internal vibrations. As was mentioned in the introduction the C_{60} molecule belongs to the highly symmetrical I_h point group. The high symmetry reduces the vibrations to be distributed among 46 different modes. The modes describe how different vibrations react to certain symmetry operations² Of the 46 vibrational modes of C_{60} , only four are infrared active ($4F_{1u}$) and ten are Raman active ($2A_g + 8H_g$). Thus the IR and the Raman spectra of C_{60} are rather simple as can be seen in figure 2.7. The simplicity stems from the high symmetry, and consequently lowering the symmetry, by for example doping, will result in a more complex spectrum where previously silent modes may be activated, and

²For a thorough explanation of the meaning of the point group assignments and irreducible representations there are many useful web-pages, like e.g. [42], and text books in chemistry and group theory, e.g. [43].

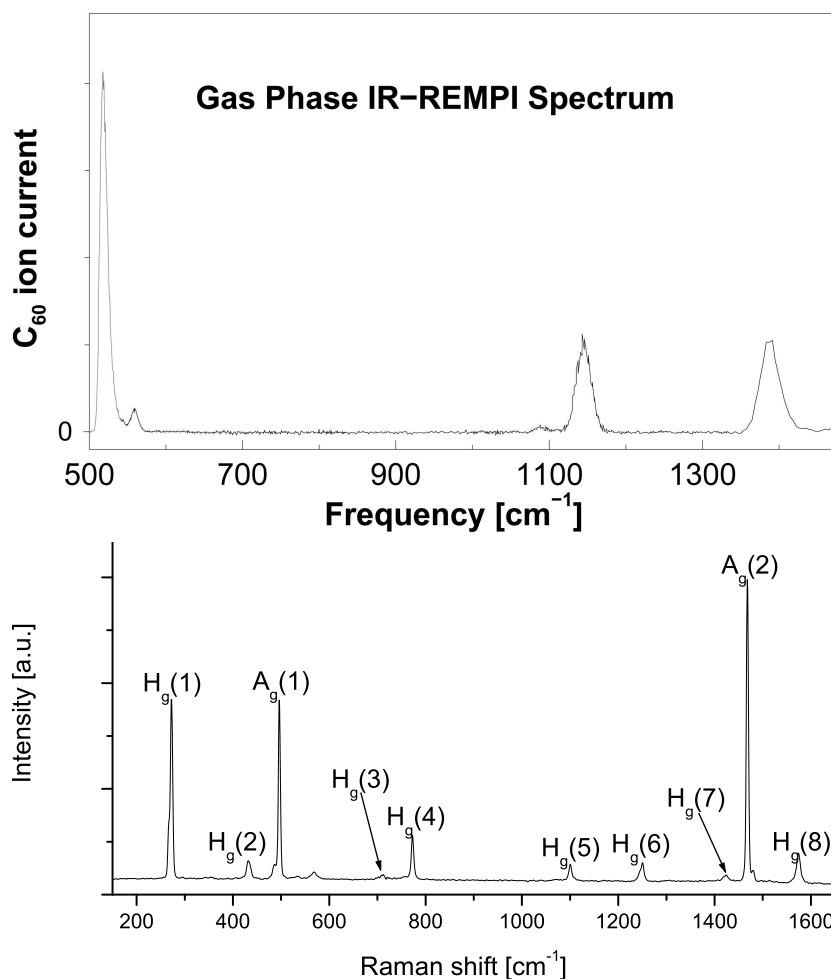


Figure 2.7: The vibrational spectra of C_{60} . The upper graph shows the IR absorptions spectrum with the four F_{1u} peaks. Graph taken from [44]. The lower graph shows the Raman spectra.

existing modes may be split or shifted in frequency. Therefore the addition of a lithium atom in the fullerene interior can significantly alter the appearance of the IR and Raman spectra if it breaks the molecular symmetry. Calculations indicate that the lithium, at least partially, donates its valence electron to the fullerene cage [45], so that the cage has a net negative charge and the lithium remains positively charged. Qualitatively the C_{60} cage can be seen as a conducting shell and the polarisation of the cage will drive the encapsulated ion to an off-centre position. So there is a potential for major changes to the vibrational spectrum. If the added atom for example would be stabilised under one of the cage hexagons, this

would change the molecular symmetry to the D_{3d} group. However, the energy differences between the various sites inside the cage where the metal ion can reside are low, only about 0.04 eV [46], so at room temperature the Li is essentially free to move in a spherically symmetric potential with its minimum 1.35–1.5 Å from the centre of the cage. [47, 48] This means that the IR and Raman spectra should remain similar to those of pristine C_{60} , with the addition in the IR spectrum of a broad band in the region 350–450 cm^{-1} , with overtones at 650–850 cm^{-1} , originating from the motion of the cation inside the cage [49], see figure 3.13.

Liquid chromatography shows (section 3.1) that the retention times for the E1 and E2 fractions of $\text{Li}@C_{60}$ overlap the C_{60} dimers and trimers respectively. The polymerised fullerene species have much more complex vibration spectra than the monomer due to the reduction of molecular symmetry. In the C_{60} dimer several hundred vibrations are Raman and IR active according to theoretical analyses [50]. So if insertion of Li into the fullerenes, as has been suggested [51], leads to the formation of dimers and possibly trimers then the vibrational spectra might be very different from the pristine C_{60} .

Also the C_{70} , with D_{5h} symmetry, shows a much more intricate vibrational spectrum than C_{60} . C_{70} has 31 infrared and 53 Raman active modes [52, 53], and it can form several stable dimer isomers with different symmetries.

To conclude, the doping of fullerenes with metal ions generally leads to rather small changes in the vibrational spectrum, unless it gives rise to polymerisation of the molecule, in which case the spectrum can look significantly different from the monomeric species.

2.5 Electron paramagnetic resonance

Electron paramagnetic resonance (EPR) or electron spin resonance (ESR), as it is frequently called, is a technique closely related to nuclear magnetic resonance (NMR). Both deal with the interaction of electromagnetic fields with magnetic moments; in the case of NMR, the magnetic moments of the nuclei, whereas EPR responds to the spin of the electrons. The principle of EPR measurements is fairly straightforward. The sample is placed in a cavity in a magnetic field and irradiated with microwaves, usually in the X-band region (~ 9 GHz). The magnetic field is varied until the splitting of the energy levels is equal to the energy of the microwave radiation. This happens when $\Delta U = g\beta_e B = h\nu$, where B is the applied magnetic field strength, β_e is the Bohr magneton, ν is the radiation

frequency, and g is the generalised electron g factor, generalised meaning that it is defined to include the effect of any local magnetic field.

The Li@C_{60} used in our measurement was prepared in bulk in a quartz ampoule and as thin films deposited on teflon substrates. The measurements were performed *ex situ* at room temperature and at 77 K on a 9.3 GHz Varian E112 EPR spectrometer. Standards of DPPH (diphenylpicrylhydrazyl) and Mg^{2+} in MgO were used for identification of EPR parameters. For comparison samples of pure C_{60} were prepared and measured in the same manner.

2.6 Conductivity of thin films

The electrical properties of fullerenes in general, and the endohedral fullerenes especially has been of interest for a long time. Several studies have been performed on the conductivity of thin films of fullerenes, but not much work has been done on endohedral fullerenes. To measure the conductivity of thin sublimed films of Li@C_{60} and La@C_{82} a setup was constructed in a small vacuum chamber that can be pumped down to 10^{-8} mbar. The setup consists of a small quartz crucible that can be heated to ca 500 °C from which the fullerenes can be evaporated onto a chip. The chip, sketched in figure 2.8, placed on a sample holder that can be heated to ca 300 °C for temperature dependent measurements, has four thin gold electrodes partially covered with silicon-oxide used for standard four-probe van-der-Pauw [54] I-V measurements. The distance between the electrodes is 150 μm , and the fullerenes are sublimed through a mica mask placed on top of the chip. The diameter of the fullerene spot is roughly 1 mm, which is much smaller than the spread of the effusive fullerene beam. This ensures a homogeneously deposited film covering the end points of the electrodes. The thickness of the deposited film is controlled by regulating the deposition time with a shutter. After the experiments the thickness is measured using a profilometer. From the I-V measurements, performed with a Hewlett Packard 4156B precision analyser, and the thickness of the film the resistivity can be determined.

For checking the effect of oxygen exposure, the vacuum pumps were stopped and the chamber was vented with ambient laboratory air. After a certain time period the valve was closed and the pumps restarted.

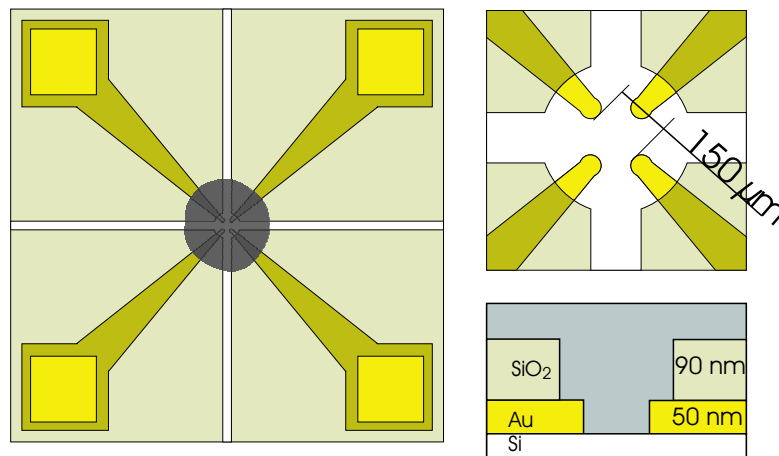


Figure 2.8: A sketch of the sample used in electrical measurements on thin fullerene films.

3

Results and Discussion

In this chapter the results of the investigations of endohedral fullerenes will be discussed.

First the separation of the endohedral fullerenes from the low-energy ion bombarded films using HPLC, which results in two different fractions of Li@C_{60} and one fraction of Li@C_{70} , is presented in section 3.1.

The different species of metallofullerenes were investigated using Raman and FTIR spectroscopic methods, as well as EPR, to try to discern the differences between them.

During the course of investigations it was noted that films of endohedral fullerenes deteriorated after some time when exposed to air, and this in much higher degree than empty fullerenes. The effect of exposure to air of thin metallofullerene films was studied using LD-TOFMS and conductance measurements. These results are presented in section 3.4.

3.1 Separation of Li@C_{60} and Li@C_{70}

In figure 3.1 a typical mass spectrum of a production film, i.e. an aluminium foil taken straight off the cylinder, after deposition of C_{60} and irradiation with Li^+

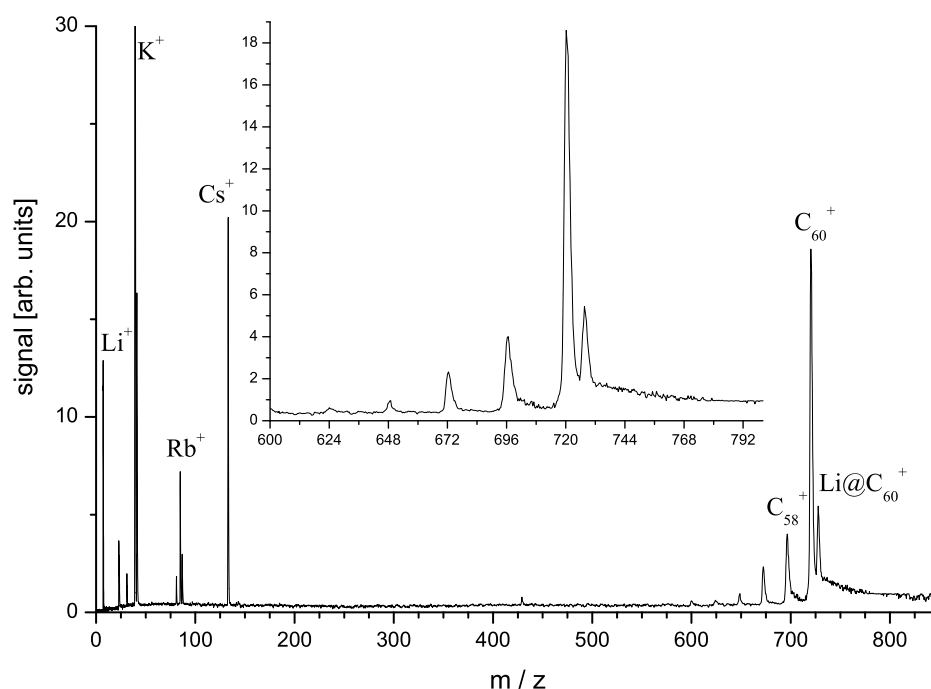


Figure 3.1: A typical mass spectrum of a production film of Li@C_{60} . Li@C_{60}^+ is clearly visible at 727 mass units. The other prominent peaks are C_{60}^+ , and the alkali metal ions Li^+ , Na^+ , K^+ , Rb^+ , and Cs^+ .

ions, and inserted into the time-of-flight mass spectrometer, is shown. In this case the film was $\sim 3500 \text{ \AA}$ thick and irradiated with 30 eV Li^+ in a ratio of 1 ion per fullerene molecule. The mass spectrum was taken using the laser desorption mode of the TOF. In the low mass end of the mass spectrum a number of peaks belonging to the alkali ions are visible. The very strong potassium signal and the sodium signal are present in all our mass spectra. The Rb^+ and the Cs^+ , however are only visible in films that have been irradiated with alkali ions, and appear to be impurities from the ion emitters [55]. The intensity of the alkali peaks does not reflect their abundance in the film. Since the alkalis have low ionisation potentials and are effectively detected by the MCPs [36] the size of these signals are exaggerated. The most prominent peak in the high mass end of the spectrum is that of C_{60}^+ at 720 atomic mass units. Preceding it are a number of peaks separated by 24 mass units. They are the product of sequential C_2 -evaporation from the parent C_{60} molecule. Trailing the C_{60} peak is a tail that originates from delayed ionisation of the C_{60} [56], a process where the energy from the laser shot is stored in vibrational modes before the molecule eventually ionises. At 727 u the peak from Li@C_{60}^+ is clearly visible. Its area is $\sim 10\%$ relative to that of C_{60} , which

gives a lowest estimate of the amount of lithiated material in the film, since the Li@C_{60} cool predominantly by losing the encaged lithium [57]. Some concern may be raised that the peak might come from exohedral Li:C_{60} instead of the endohedral metallofullerene. It is however known that exohedrally attached lithium binds only weakly to the fullerene cage, a binding energy of 2.2 eV has been calculated [58]. The ionisation energy for Li@C_{60} is calculated to 6.1 eV [59], so any exohedral Li:C_{60} will break apart before ionising. Furthermore, studies on films consisting of a mixture of lithium metal and C_{60} show no, or extremely small, amounts of Li:C_{60} , even if significantly more lithium is present.

As described in section 2.2 the production film is dissolved in CS_2 in an ultrasonic bath. The majority of the material on the film is dissolved, but usually an insoluble part of 10–15 % by weight is left after filtration. LD-TOFMS on the insoluble material shows strong alkali peaks, C_{60} , and many peaks probably from carbon compounds up to a few hundred u. The spectra also show some amount of LiC_{60} . Presumably the LiC_{60} and the C_{60} are in the form of polymerised species formed during the irradiation, but subsequently broken apart in the laser desorption process. The amount of insoluble material increases if the ratio of ions to fullerenes is higher than the usual one ion per C_{60} .

The soluble material is dried and redissolved in DCB, which is used as eluent in the HPLC process. As the solution emerges from the HPLC column the absorption is monitored over the wavelength interval 290–800 nm every 6 seconds. A typical spectrum can be seen in figure 3.2. The UV-VIS spectroscopic analysis allows conclusions to be drawn about the electronic structure of the different fullerene species. This has been discussed earlier by Gromov and co-workers [51], see section 3.2.1.

The absorption at 340 nm is plotted against the retention time for monitoring the separation in the column. 340 nm is strongly absorbed by most fullerene species. In C_{60} the strong dipole transition between the HOMO-1 and the LUMO lies at approximately this wavelength. The acronyms HOMO and LUMO stands for Highest Occupied Molecular Orbit and Lowest Unoccupied Molecular Orbit respectively. In figure 3.3 the absorption at 340 nm for some different samples are compared. We can see that about nine minutes after insertion into the column C_{60} emerges. The smaller peak before the C_{60} comes from the solvent. After twelve minutes another peak appears in the absorption spectrum. This species gives a mass peak at 727 u, Li@C_{60} , in LD-TOFMS, and has been dubbed E1. Yet another species appears after 17.5 min, which also gives a Li@C_{60} peak in the TOF. Consequently the fraction collected at this retention time is referred to as E2.

In order to learn more about what structure the fractions E1 and E2 have, their

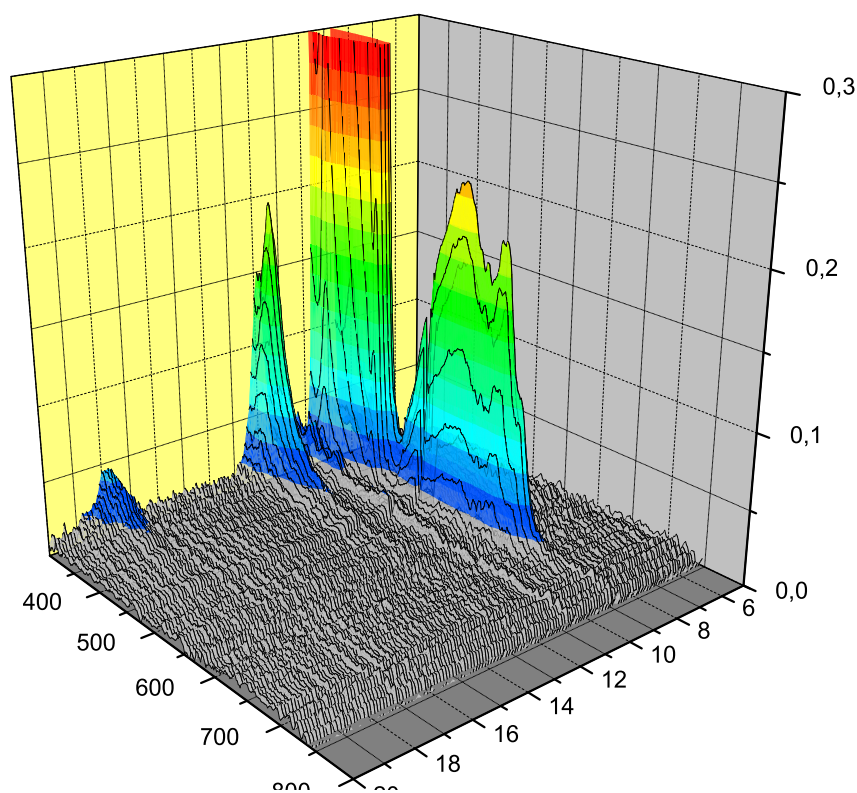


Figure 3.2: A typical absorption chromatogram from a production film. The absorption is monitored every 6 seconds over the wavelength interval 290–800 nm.

retention times were compared with other fullerene species. In figure 3.3 the dotted line is the absorption from a sample of C_{60} ball-milled with metallic lithium. This sample is known to contain dimers and trimers of C_{60} [41]. As can be seen, the retention time of the dimeric species, $(C_{60})_2$, nicely overlaps the first endohedral fraction. The E2 peak appears at the same time as the trimer peak in the ball-milled sample. However the trimer fraction consists of several peaks spread out over a longer time than the endohedral fraction. This is because several stable isomers exist of $(C_{60})_3$ and they may have different retention times. It seems likely that if E2 really is a trimer it will consist predominantly of one isomer.

For production of $Li@C_{70}$, the procedure is the same as for $Li@C_{60}$. In the HPLC analysis C_{70} exits the column after 10.5 minutes, i.e. slightly later than the relatively inert C_{60} . After 19 minutes the only fraction that gives $Li@C_{70}$ in LD-TOFMS emerges. This is clearly different from the $Li@C_{60}$ with its two endohedral fractions. However, similarly to $Li@C_{60}$ the lithiated species of C_{70} emerges from the column after the same retention time as the C_{70} dimer.

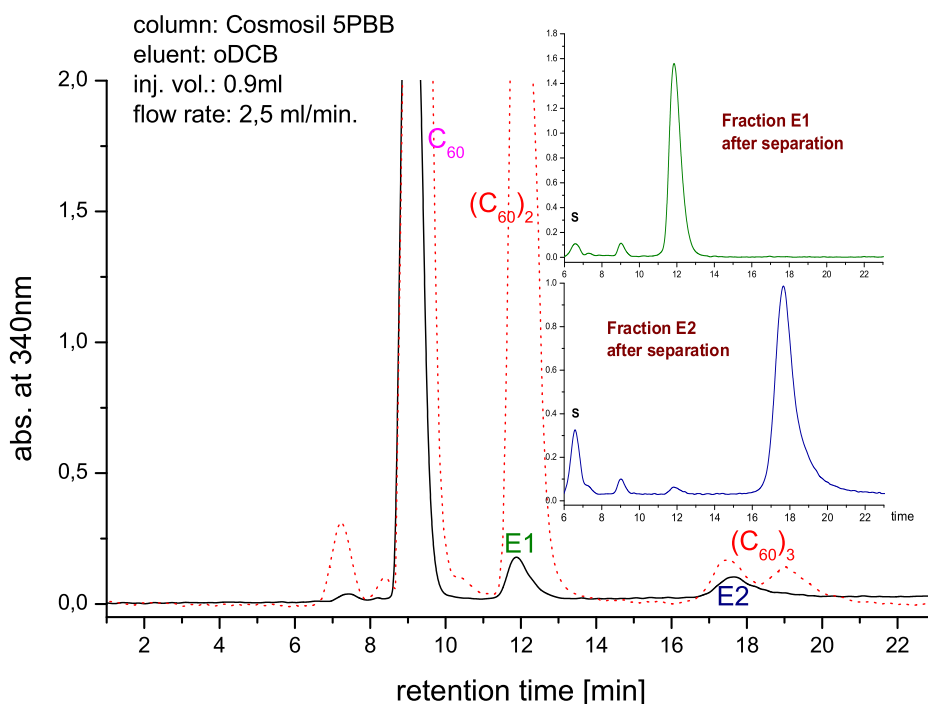


Figure 3.3: Absorption at 340 nm monitored as a function of retention time for different fullerene samples. The solid line is a chromatogram from a production film of $\text{Li}@C_{60}$, and the dotted is from C_{60} ball-milled with metallic lithium. The inserts show chromatograms of the purified fractions E1 and E2.

3.1.1 Production of $\text{Na}@C_{60}$ and $\text{K}@C_{60}$

There was also attempts made to produce and purify other alkali metallofullerenes using the same methods as for $\text{Li}@C_{60}$. As was mentioned above (sec. 2.1.1) the thresholds for production of $\text{Na}@C_{60}$ and $\text{K}@C_{60}$ are higher than for $\text{Li}@C_{60}$, being 18 eV and 40 eV respectively [25]. LD-TOFMS investigation of ion irradiated C_{60} films show a maximum in the $X@C_{60}^+$ peak at 70 eV ion energy for Na^+ and 85 eV for K^+ [29]. The capture window of both the LD-TOFMS and gas phase investigations coincide perfectly, so there is little doubt that endohedral fullerenes really are created.

We have performed ion bombardment experiments with both Na^+ and K^+ . LD-TOFMS on the production films shows a small peak at 759 amu for the potassium irradiated films. However, the amount of insoluble material in the irradiated films is much higher than for $\text{Li}@C_{60}$ production. Using K^+ ions at 85 eV results in $\sim 50\%$ insoluble material. The reason is the higher ion energy that increases the

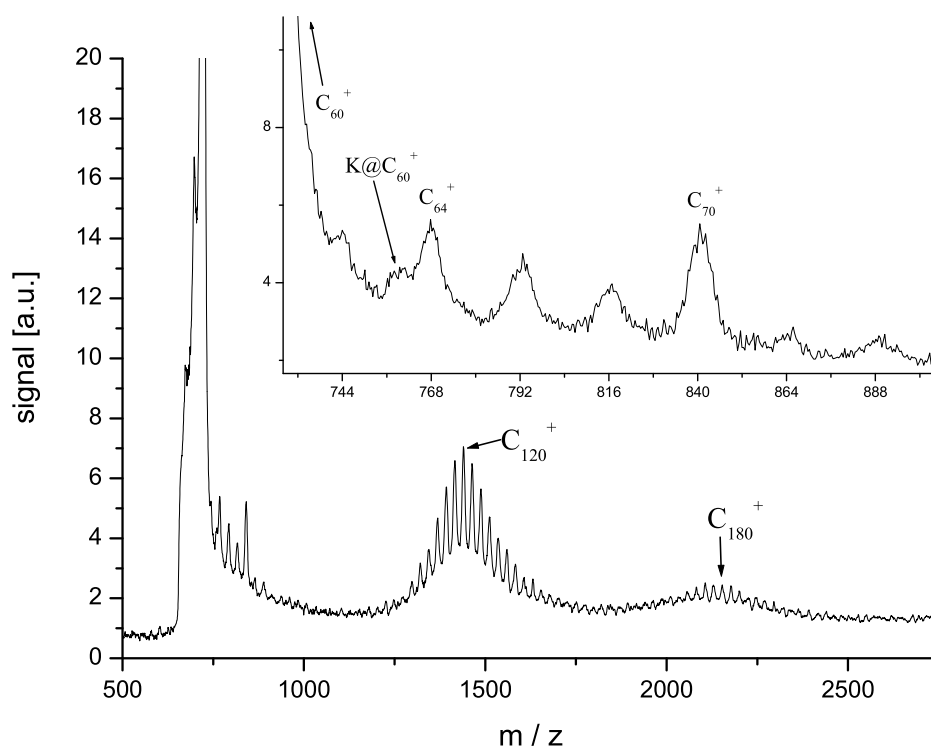


Figure 3.4: Mass spectrum of a production film of $\text{K}:\text{C}_{60}$ prepared with an ion energy of 85 eV. The ions at higher masses are due to coalescence in the the desorption plume.

destruction and polymerisation of the fullerenes.

Mass spectrometry of $\text{K}@\text{C}_{60}$ is difficult. The very intense K-peak saturates the detector if the normal LD setup is used. By inserting an extra grid between U2 and ground in figure 2.6 and keeping U1 on ground, we let the ions drift to the first grid. This way, most of the potassium ions have passed through the extraction region before the field is pulsed. The mass spectrum in figure 3.4 is taken on a production film of $\text{K}:\text{C}_{60}$ produced with an ion energy of 85 eV, and the ions drifted for $80 \mu\text{s}$ before the fields were pulsed. The C_{60} peak seen at the left-hand side is cut, but stretches to over 100 units height and completely dominates the spectrum. A small, but clearly visible peak of KC_{60} can be found at 759 u. The peak is very small compared to $\text{Li}:\text{C}_{60}$ films, the ratio $\text{KC}_{60}/\text{C}_{60}$ is only about 1%. Using the same arguments as for Li, one can assume that the chance of surviving the high internal energies involved in the LD process should be low for exohedral fullerenes. However, unlike for $\text{Li}:\text{C}_{60}$, exohedral KC_{60} are not uncommonly found in laser desorption of potassium containing film. It is thus uncertain whether the peak at

759 u really represents endohedrally doped fullerenes.

We also see in the spectrum groups of peaks separated by 24 mass units around 1440 u and also around 2160 u. These are products of coalescence of fullerenes in the laser plume, and have been observed in earlier LD experiments [60, 61]. However, these peaks are not normally detected in our LD experiments on C_{60} and $Li@C_{60}$. Clearly the potassium ion bombardment increases the level of coalescence, but through which mechanism is not known. Perhaps fragmentation of the fullerenes during ion bombardment plays a role, as it has been shown that fragments are important for the formation of coalesced fullerenes [60]. Oxygen can also increase the coalescence probability of C_{60} , as was demonstrated for $C_{60}O_n$ ($n = 1, 2, 3$) prepared by ozone treatment [62]. We show in section 3.4 that metallofullerenes exposed to oxygen show similar behaviour as C_{60} after ozone treatment and UV activation of oxygen. This increased reactivity might have influence, but it does not explain the absence of coalescence in $Li@C_{60}$. This is still an open question and must be investigated further.

The soluble portion of the $K:C_{60}$ films has been investigated using HPLC, and the chromatogram is similar to that of $Li@C_{60}$, with two fractions appearing after the empty C_{60} . However, the ratio of E2 to E1 is much smaller for $K:C_{60}$, and the E2 peak shows a bimodal form not seen in $Li@C_{60}$, but very similar to the trimer fraction in the ball-milled sample (see fig. 3.3). LD-TOFMS investigation of the separated fractions shows no $K@C_{60}$, so any endohedral material produced is apparently not soluble in CS_2 . However, material dissolved in aniline does show a peak of KC_{60} in the mass spectrometer, as well as C_{60} and C_{70} and a very high K peak. It is thus also in this case uncertain whether the KC_{60} peak is of endohedral nature or not.

Experiments were also performed with sodium, but since $Na@C_{60}$ has almost the same mass as C_{62} , adding an element of uncertainty to mass spectrometric investigations, we have focused our attention on potassium instead.

3.2 Spectroscopy on metallofullerenes

3.2.1 UV-Vis spectroscopy of $La@C_{82}$

As described in section 3.1 UV-Vis spectroscopy over the range 300-800 nm is performed on every species exiting the HPLC column. The UV-Vis spectra of the endohedral lithium species have been measured previously and are discussed in detail by Gromov *et al.* [51].

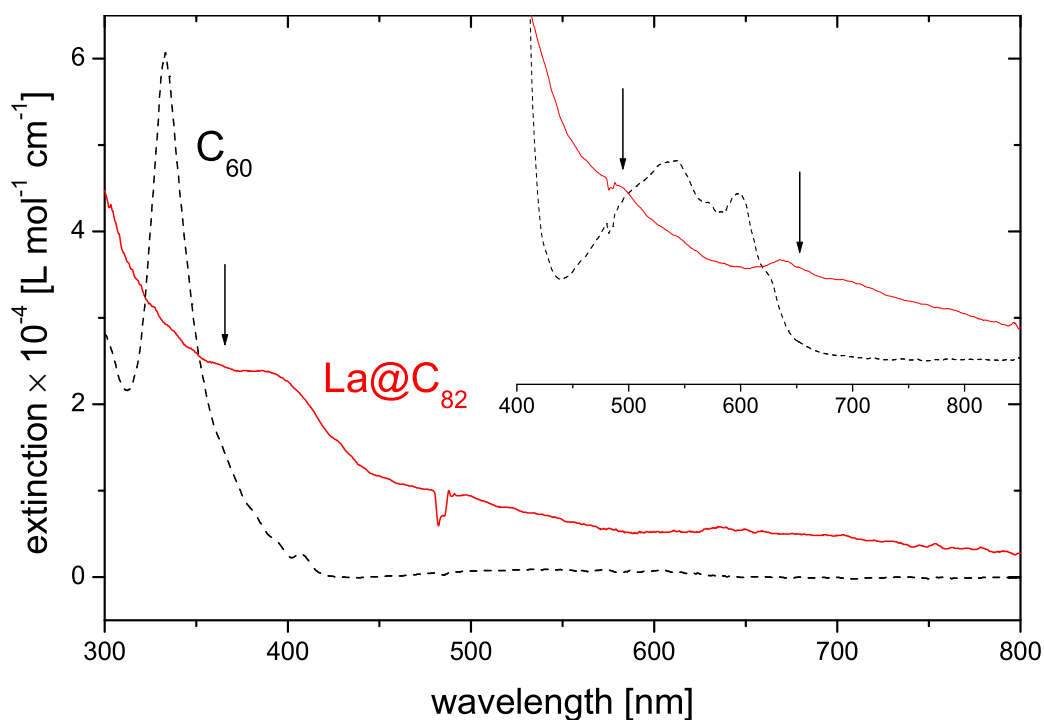


Figure 3.5: UV-vis spectra measured on C_{60} (dashed) and $La@C_{82}$ (full) in DCB. The insert show the structures in the middle of the spectral range (with shifted intensities for clarity). The dip at 484 nm is an instrumental artifact. Taken from [31].

The UV-Vis spectrum of $La@C_{82}$ was measured by Lassesson and co-workers [31] using the spectrometer in the HPLC setup. Solutions of $La@C_{82}$ and C_{60} in DCB with concentration $(9 \pm 3) \times 10^{-5}$ mol/L were prepared and sent through the spectrometer. The extinction ϵ , defined by $A = \epsilon xc$, where A is the absorption, x the optical pathway and c the concentration in mol/L, was calculated. The result is plotted in figure 3.5. Marked with arrows in the figure are transitions between molecular orbitals in $La@C_{82}$ measured by UV-photoelectron spectroscopy and scanning tunneling spectroscopy [63]. They show good agreement with features in the measured UV-Vis spectrum.

For comparison with the UV-Vis measurements in solution, thin films of $La@C_{82}$ and C_{60} were prepared by evaporation on glass substrates. Several samples with different thickness were made and the absorption was measured using the same spectrometer as in the experiments described above. The thickness of the samples was measured using a profilometer.

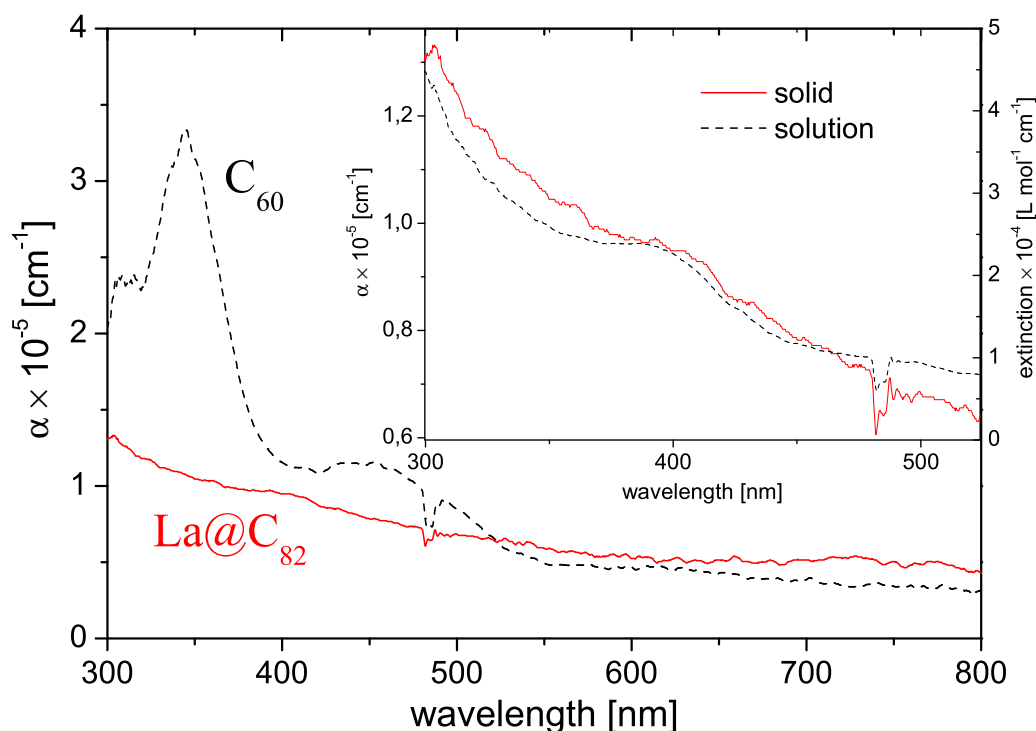


Figure 3.6: The UV-Vis spectra of C₆₀ and La@C₈₂ deposited on glass substrates. The inset shows a comparison of the spectra for La@C₈₂ in solution and on a substrate.

The absorbance, defined by the expression $I = I_0 e^{-\alpha d}$, where d is the thickness of the film, I is the transmitted and I_0 the incident light, is plotted in figure 3.6. The spectrum for C₆₀ is in good agreement with earlier measurements [64], but no spectra of La@C₈₂ on substrates could be found in the literature.

There are some differences between the spectra of C₆₀ taken in solution and on substrates. For C₆₀ the prominent absorption peak at 335 nm is shifted by about 11 nm in the solid spectrum. Also, the absorption band from 420 nm has much higher intensity in the spectrum on a substrate. The features in the solid spectra are also broader than in solution. These differences can be explained by induced dipole interaction of neighbouring molecules, something that can lead to broadening of the molecular orbitals [6]. The solid state spectrum of La@C₈₂ is very broad and shows almost no details, the resonance at 400 nm is the only one that can be resolved, and it is shifted by some 10 nm. The thin La@C₈₂ films are, as we shall see in section 3.4, sensitive to air. There was unfortunately no possibility to make the measurements in inert atmosphere (e.g. a glove-box) which is why

we can not eliminate the possibility of oxidation of the metallofullerenes. This would undoubtedly affect the absorption spectrum.

3.2.2 Vibrational spectrum of Li@C₆₀

The infrared absorption spectra of the two chromatographically separated fractions of Li@C₆₀ are shown in figure 3.7. For comparison also the spectrum for the [2 + 2] dimer (C₆₀)₂ (depicted in figure 3.9) is displayed in the top panel. The positions of the active vibrational modes of pristine C₆₀ (526, 576, 1183, and 1429 cm⁻¹ [6])¹ are marked with stars are.

One can immediately see that the spectra of the lithiated species are much closer to that of the dimer than to pristine C₆₀. Most of the absorption bands of the endohedral fractions correspond to bands of the dimer, even though some variations in the relative intensities can be observed. But there are also a number of peaks in the spectra of both endohedral fractions that don't have any counterparts in the (C₆₀)₂. These peaks are marked with arrows in figure 3.7b and are located at 746, 1034, 1376, 1455, and 1699 cm⁻¹. These peaks are thus presumably due to the insertion of Li into the C₆₀. This is also in qualitative agreement with theoretical calculations of the IR absorption of Li@C₆₀. [58] A strong indication of the endohedral nature of the lithiated fullerenes is the absence of a strong absorption band at 440 cm⁻¹ predicted for exo- but not endohedrally doped C₆₀ [58].

The spectra from the Raman measurements on the chromatographically isolated metallofullerenes are shown in figure 3.8, together, for comparison, with the spectra of pristine C₆₀ and the [2 + 2] dimer. The ten active Raman modes in C₆₀ are, as mentioned above, divided into two non-degenerate, and eight five-fold degenerate states. The non-degenerate modes are the “radial breathing mode” (*A_g*(1)) at ca 495 cm⁻¹ and the “pentagonal pinch” mode (*A_g*(2)) at 1470 cm⁻¹. They are highly symmetrical and easy to visualise. The breathing mode is the radial displacement of all the carbon atoms whereas the pinch mode is a tangential motion of the atoms, expanding the hexagons and pinching the pentagons. The degenerate modes are more complicated (see [65]). When the molecular symmetry is altered due to doping or polymerising one can expect that the degeneracy of the *H_g* vibrations will be lifted and that those modes will split into several peaks. The non-degenerate modes, on the other hand, will respond to disturbances mainly by shifting to higher or lower frequencies. In particular the *A_g*(2) mode is very sen-

¹Some nice animations of the vibrations of C₆₀ have been put on the Internet by Menéndez and Page [65].

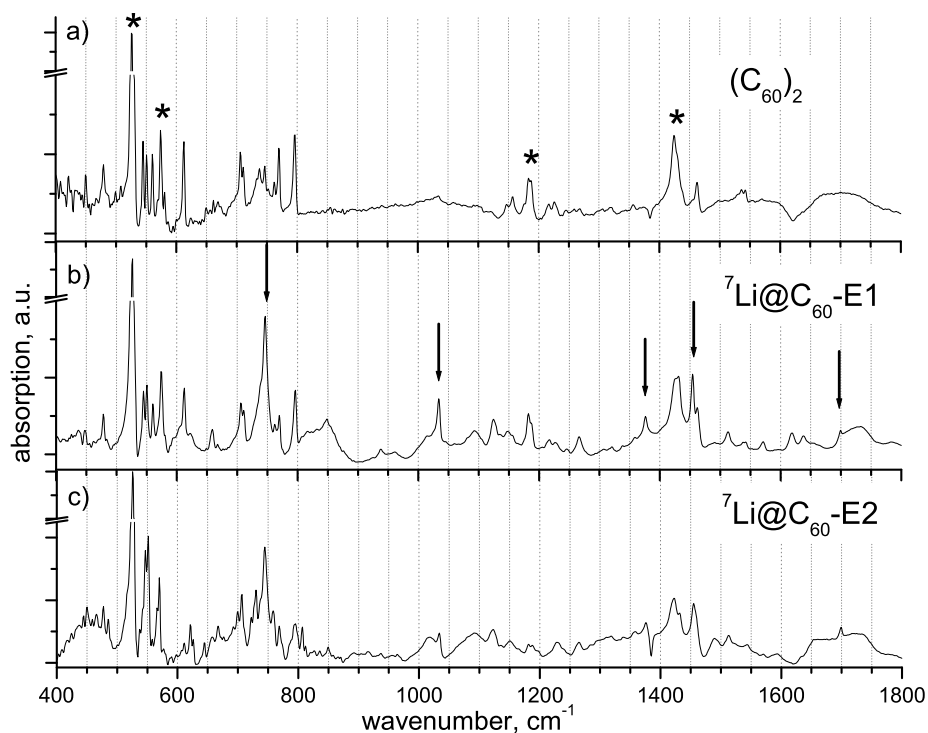


Figure 3.7: The FTIR spectra of the two chromatographically separated fractions of Li@C_{60} and the $(\text{C}_{60})_2$ dimer. The stars in the top figure show the absorption peaks of pristine C_{60} . The arrows mark new peaks in the endohedral spectra.

sitive to charging of, or bonding to the cage. One additional electron or covalent bonding will shift the peak $6\text{--}9\text{ cm}^{-1}$ to lower frequencies [6, 66].

In our measurements the $A_g(2)$ mode is red-shifted about 5 cm^{-1} in the dimer and the $\text{Li@C}_{60}\text{-E1}$ compared to the C_{60} spectrum. When comparing the E1 and the $(\text{C}_{60})_2$ spectra one can see that there is great similarity between them. And much more so than between E1 and the pristine C_{60} , just as in the IR measurements. In particular the splittings of the $H_g(1)$ and the $H_g(2)$ modes are practically identical. Also the breathing mode, $A_g(1)$, corresponds well, even if there is a slight tendency for splitting of this mode into two components. This is somewhat unexpected. New, weak features can be seen around 350 cm^{-1} and at $100\text{--}150\text{ cm}^{-1}$, but only the lower of these is present in the E2 spectrum. Therefore it is not as straightforward to assign any peaks to the effect of lithium insertion as in the case

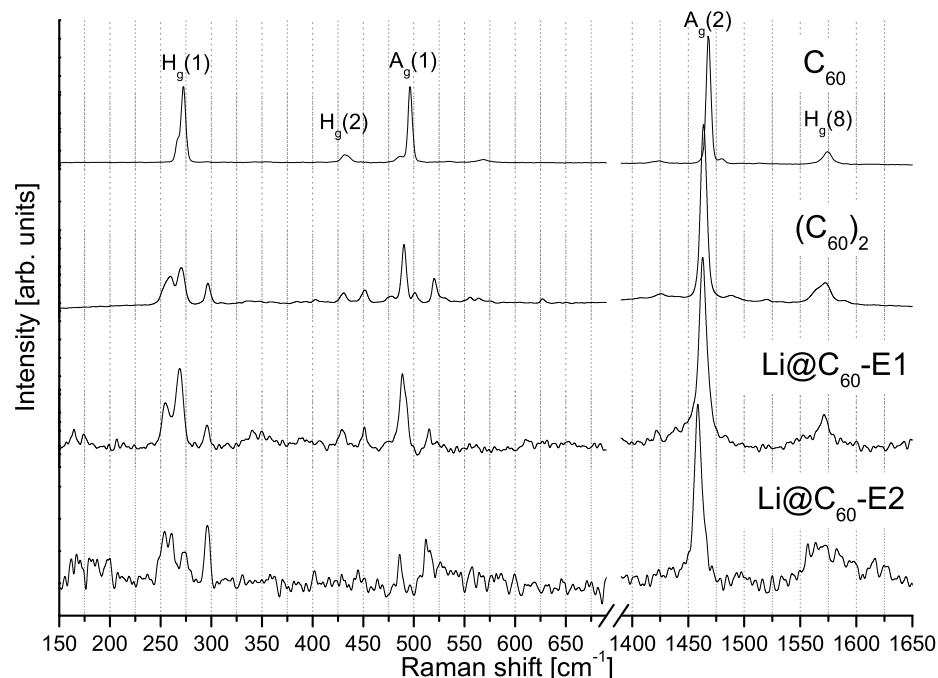


Figure 3.8: Raman spectra of the endohedral fractions $\text{Li@C}_{60}\text{-E1}$ and $\text{Li@C}_{60}\text{-E2}$, together with the spectra of C_{60} and the dimer $(\text{C}_{60})_2$.

of IR absorption.

Taken together, the strong similarity between the vibrational spectra of the $\text{Li@C}_{60}\text{-E1}$ fraction and the $[2 + 2]$ dimer $(\text{C}_{60})_2$ both in infrared and in Raman spectroscopy, and also the retention time overlap of the two species in HPLC implies that one can with certainty assign the E1 fraction as the dimer $(\text{Li@C}_{60})_2$. The question is the type of binding between the two carbon cages in the dimer. Theoretical investigation shows that the most stable form of neutral $(\text{C}_{60})_2$ is the 66/66 isomer of the $[2 + 2]$ cycloadduct [67, 68], which is the phase formed by e.g. the mechanochemical process used to produce our $(\text{C}_{60})_2$ [41]. The single-bonded dimer on the other hand is predicted to be unstable for the neutral molecule [67, 68]. For negatively charged fullerene cages the opposite situation holds, the theoretical calculations show the single-bonded dimer as slightly more stable than the double-bonded cycloadduct. This is corroborated by x-ray powder diffraction of exohedrally doped A_1C_{60} [69, 70], where the alkali atoms donate an elec-

tron to the fullerene, and by investigation of the azafullerene $(C_{59}N)_2$, which is isoelectronic to $(C_{60}^-)_2$ [71]. Despite great similarity between the Raman and IR spectra of the single- and double-bonded dimers, group theoretical analysis predicts 174 Raman active modes for either type and 174 contra 132 IR active modes for the single-bonded (C_{2v} symmetry) and double-bonded (D_{2h}) respectively², there are some telltale differences. Strong bands at 448 and 625 cm^{-1} have been observed for single-bonded $(C_{59}N)_2$ and $(C_{60}^-)_2$ but are not observed for the cycloadduct [71]. In the IR spectra a strong line at ~ 795 is present in the double-bonded [50, 72], but not in the single-bonded [73] dimer. The presence of this mode and the absence of the aforementioned Raman modes implies that the Li@C₆₀-E1 fraction is a [2 + 2] dimer.

Comparing the two Li@C₆₀ fractions one notices that the IR spectrum of the E2 fraction in figure 3.7 has less pronounced features than the E1, particularly in the region above 900 cm^{-1} . There are also distinct differences in the splitting of the peaks around 550 cm^{-1} , derived from the $F_{1u}(1)$ and $F_{1u}(2)$ modes. Here, as expected, the E1 is very similar to the dimeric sample, whereas the E2 is markedly different. Also in the Raman measurements (fig. 3.8) one finds dissimilarities. The E2 spectrum gives a more complex appearance than does the E1, something that can be indicative of a lower molecular symmetry. Since the HPLC retention time for E2 overlaps the C₆₀ trimers it is not an unreasonable suspicion that it might be of trimeric nature. Comparing the measured Raman activity of our sample with calculations, performed by Porezag *et al.* [74], for different fullerene oligomers gives compelling evidence that this is indeed the case. Compared with the $(C_{60})_2$ dimer the pentagonal pinch peak is shifted 5 cm^{-1} towards lower frequencies. This shift, and the splitting of the $H_g(1)$ mode into four peaks such that the highest and lowest frequency components have the same intensity is a signature of the closed triangle structure that can be seen in figure 3.9.

A table with all the observed infrared and Raman modes of the endohedral Li@C₆₀ compared with C₆₀ and $(C_{60})_2$ together with possible band assignments can be found in Paper II.

3.2.3 Vibrational spectrum of Li@C₇₀

The FTIR vibrational spectrum of Li@C₇₀ can be seen in figure 3.10 in comparison with the spectra of the pristine C₇₀ molecule and of the dimer $(C_{70})_2$ measured by Lebedkin *et al.* [75]. Analogously to the case with Li@C₆₀, the vibrational spectra

²Due to the weak intensity and overlap between components of the same split C₆₀ modes the experimentally detected peaks are much fewer.

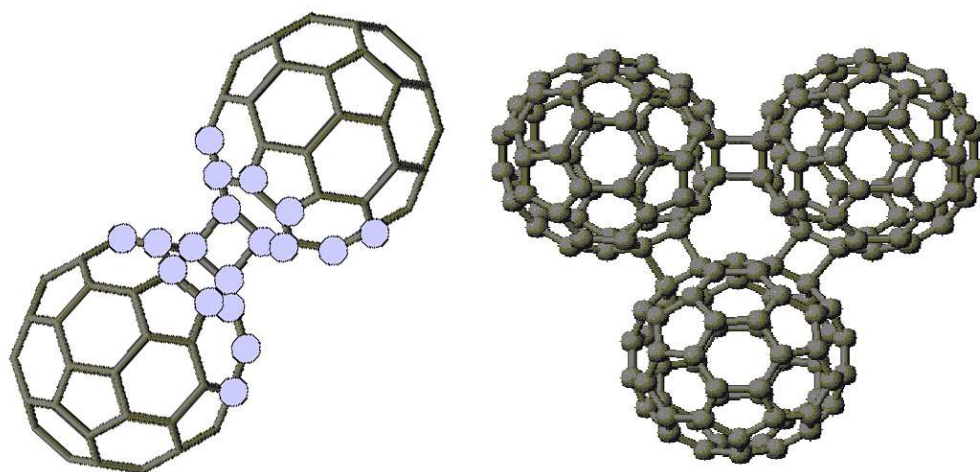


Figure 3.9: Proposed structure of the investigated endohedral species. On the left the $[2+2]$ C_{60} dimer, with circles marking the atoms strongly participating in the IR absorption mode at 796 cm^{-1} . On the right the optimised closed triangle structure from ref. [74].

of the lithiated species and the dimer of C_{70} are far closer than are the $\text{Li}@C_{70}$ and the monomeric species. Arrows in the figure mark a number of absorption bands that appear only in the lithiated sample. These are located at 734 , 745 , 1015 , and 1253 cm^{-1} . Also in the interval $400\text{--}500\text{ cm}^{-1}$ a broad absorption band can be noted. As in the case of C_{60} absorption in this region may be due to the motion of the lithium encaged by the C_{70} (see section 3.2.4).

The Raman spectrum of $\text{Li}@C_{70}$ is very similar to the spectrum of the C_{70} dimer as can be seen in figure 3.11. There are some differences in the strength of individual band, and the lithiated compound shows a shift of some $2\text{--}5\text{ cm}^{-1}$ towards lower wavenumbers. This could perhaps be due to the extra charge on the cage donated by the lithium atom.

All in all, with the excellent agreement between Raman and FTIR spectra of $\text{Li}@C_{70}$ and $(C_{70})_2$ and the overlapping HPLC retention time of these two compounds, one can conclude that $\text{Li}@C_{70}$ is of dimeric nature. The exact form of this dimer is, however, a very daunting task to determine. Five different $[2+2]$ dimers, with very similar formation energy but differing orientations of the monomeric constituent to the double bond bridge, exist for the neutral C_{70} [75]. Additional complication comes from the charge donation by the encapsulated lithium that can be, as demonstrated in the case of $\text{Li}@C_{60}$, significant for the stability of different isomers. Very few experimental investigations into negatively charged C_{70} dimers have been performed. So, while the exact structure of $\text{Li}@C_{70}$ remains elusive,

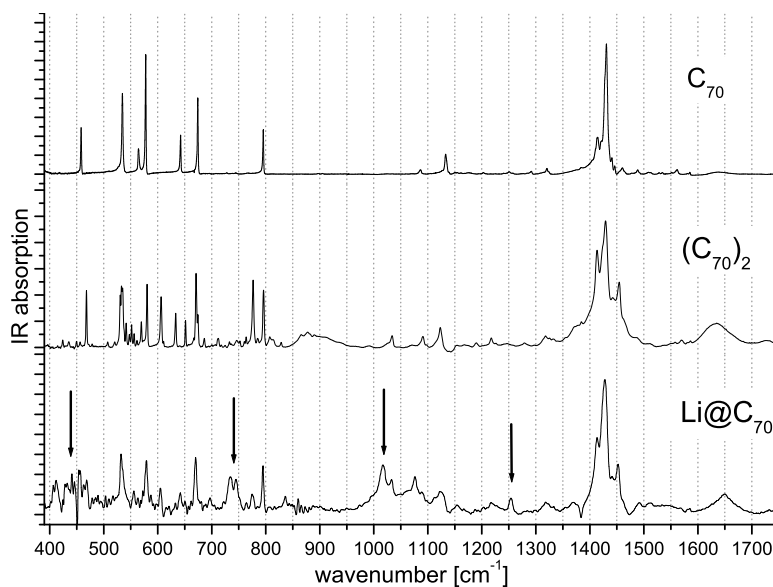


Figure 3.10: FTIR spectra of C₇₀, the dimer (C₇₀)₂ and the endohedral fullerene Li@C₇₀. The arrows mark absorption bands appearing as an effect of lithium insertion.

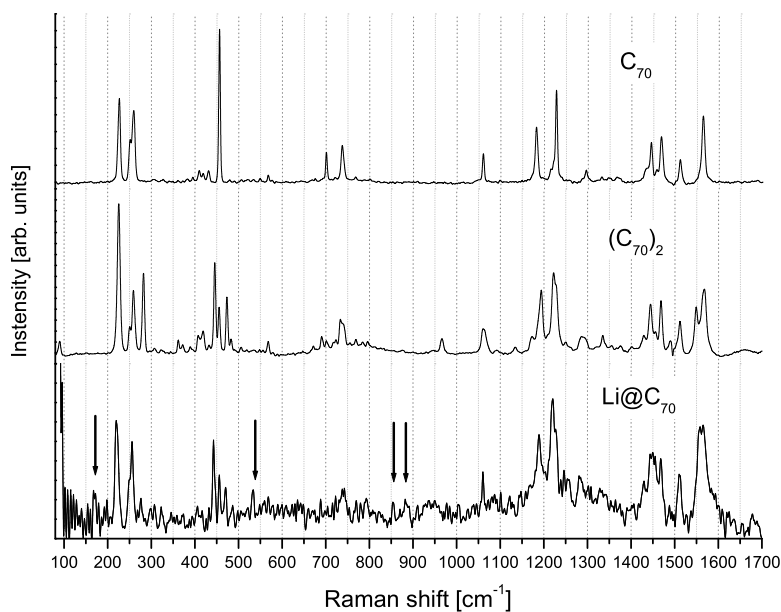


Figure 3.11: Raman spectrum of Li@C₇₀ together with spectra pristine C₇₀ and the dimer (C₇₀)₂. Arrows mark new lines appearing after lithium insertion.

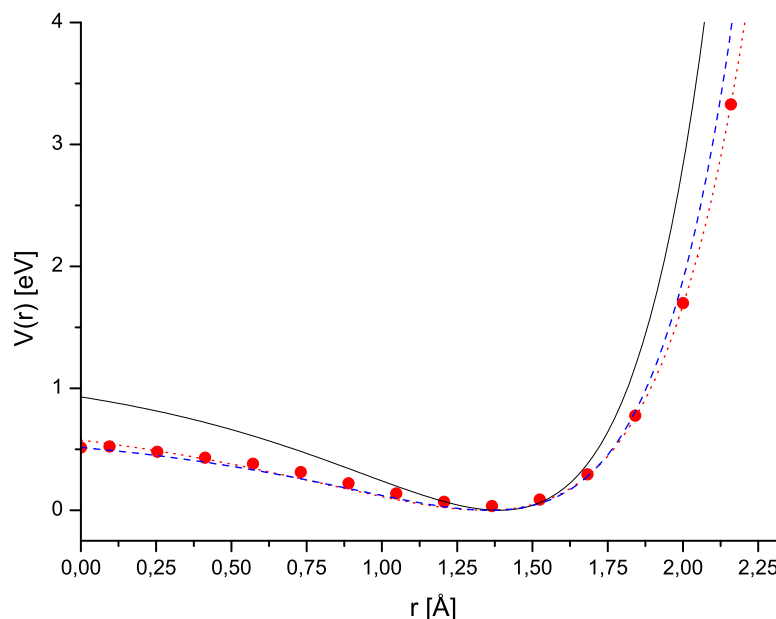


Figure 3.12: The potential for the lithium atom inside a C_{60} cage. The dashed line is the potential calculated by Dunlap *et al.* [47]; the circles are calculated by Delaney and Greer [48] and the dotted line is a fit to that data using the Morse potential in eq. 3.1. The solid line is a Morse potential with $D = 1.2$ eV.

the designation as a dimer is based on cogent evidence.

3.2.4 Motion of the encapsulated atom

As pointed out in section 2.4.1 internal doping of the fullerene is not expected to influence the vibrational spectrum significantly, but the motion of the encaged atom should give rise to an absorption band. The potential surface on which the lithium ion moves can be well approximated with the so called “reflected” Morse potential (see figure 3.12)

$$V(r) = D \left(1 - e^{a(r-r_0)}\right)^2. \quad (3.1)$$

The values of the parameters have been calculated by Dunlap *et al.* [47] to $D = 0.666$ eV, $a = 1.54 \text{ \AA}^{-1}$, and $r_0 = 1.36 \text{ \AA}$. A more recent calculation by Delaney and Greer [48] reached a very similar result as can be seen in the figure 3.12. Using the potential calculated by Dunlap *et al.* Joslin *et al.* [49] predicted

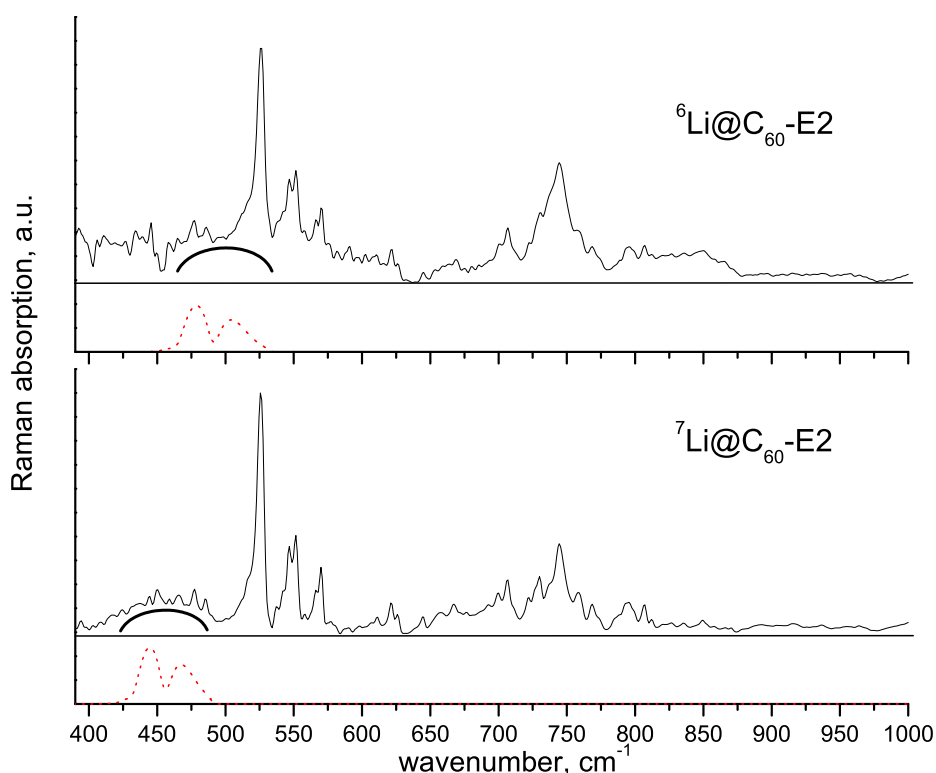


Figure 3.13: FTIR spectra for the E2 fractions of the metallofullerenes ${}^6\text{Li}@C_{60}$ and ${}^7\text{Li}@C_{60}$. The dashed lines are calculated rotation-vibration bands using the reflected Morse potential with $D = 1.2$ eV.

vibration-rotation bands at $350\text{--}450\text{ cm}^{-1}$ with overtones at $700\text{--}850\text{ cm}^{-1}$ for ${}^7\text{Li}^+@C_{60}$. The band positions for the lighter lithium isotope shift somewhat upwards.

In order to reveal which bands correspond to the motion of the internal atom, samples of metallofullerenes were prepared where different isotopes of lithium had been used in the ion bombardment. Comparing the IR-absorption spectra of the samples shows that the five new absorption peaks that appear after lithium insertion, and are marked with arrows in figure 3.7, retain their positions. They are thus not directly caused by the encaged lithium, but are due to charge transfer to the fullerene cage and distortion of the cage structure. However, broad weak absorption bands can be seen around 450 cm^{-1} in the spectrum of ${}^7\text{Li}@C_{60}\text{-E2}$, and shifted about 50 cm^{-1} to 500 cm^{-1} for the ${}^6\text{Li}@C_{60}\text{-E2}$ sample. This is at higher wavenumbers than the calculations predict, and one must assume a deeper potential well for the lithium to move in, with $D \approx 1.2$ eV, to get correct position

for the vibration-rotation bands, as can be seen in the plot in figure 3.13. One must bear in mind though, that the shift of the bands for the two isotopes is reproduced in calculations using the potential of Delaney and Greer, even if the absolute positions are somewhat displaced. One should take into account that the calculations are made for isolated molecules, and not the dimeric and trimeric species present in our samples.

To adequately investigate the motion of the internal lithium atom in the fullerenes one should preferably measure on isolated molecules, which might prove excruciatingly difficult, and at very low wavenumbers, below 100 cm^{-1} that were restricted to us due to instrumental limitations, where both Joslin *et al.* and more sophisticated models [76] predict strong rotation bands.

3.3 EPR measurements on Li@C_{60}

A pristine C_{60} molecule has no unpaired electrons and should therefore not give rise to any EPR signal. However very often two lines are still observed. These lines, the first with a g value of 2.0025 and the other closer to 2 are usually ascribed to the positively charged C_{60}^+ [77], and the negatively charged C_{60}^- [78] respectively. These lines are the results of defects where a fullerene molecule has lost an electron or bound an extra electron. The EPR resonances are narrow with a line width less than 2 G, which means that the extra electron, or hole, is delocalised over the whole C_{60} cage.

Measurements on endohedral fullerenes often reveal a number of EPR lines coming from hyperfine coupling between the nuclear spin of the encaged atom and electrons donated to the carbon cage. However, most of these measurements have been performed on M@C_{82} , with $\text{M}=\text{La}, \text{Sc}, \text{Y}$. In the case of Li@C_{60} one electron is donated to the fullerene cage, and the interaction of this unpaired electron with the nuclear moment of the Li nuclei ($I = 3/2$) should produce four closely spaced lines in the EPR spectrum.

In our measurements on C_{60} one single line was observed at $g = 2.0025 \pm 0.0005$, the line associated with C_{60}^+ . The line from C_{60}^- was not observed, but this is not very surprising; The positive line is much more commonly observed than the negative [6]. From the area of the resonance line the concentration of paramagnetic centres (N_{PC}) can be calculated. For C_{60} the concentration was on the order of 10^{17} spin/g, or roughly 1 defect in 5000 molecules. The width of the line, ΔH , both for room temperature measurements and at 77 K, is 1.2–1.5 G, which is consistent with earlier results. In figure 3.14 the peak-to-peak amplitude of the EPR

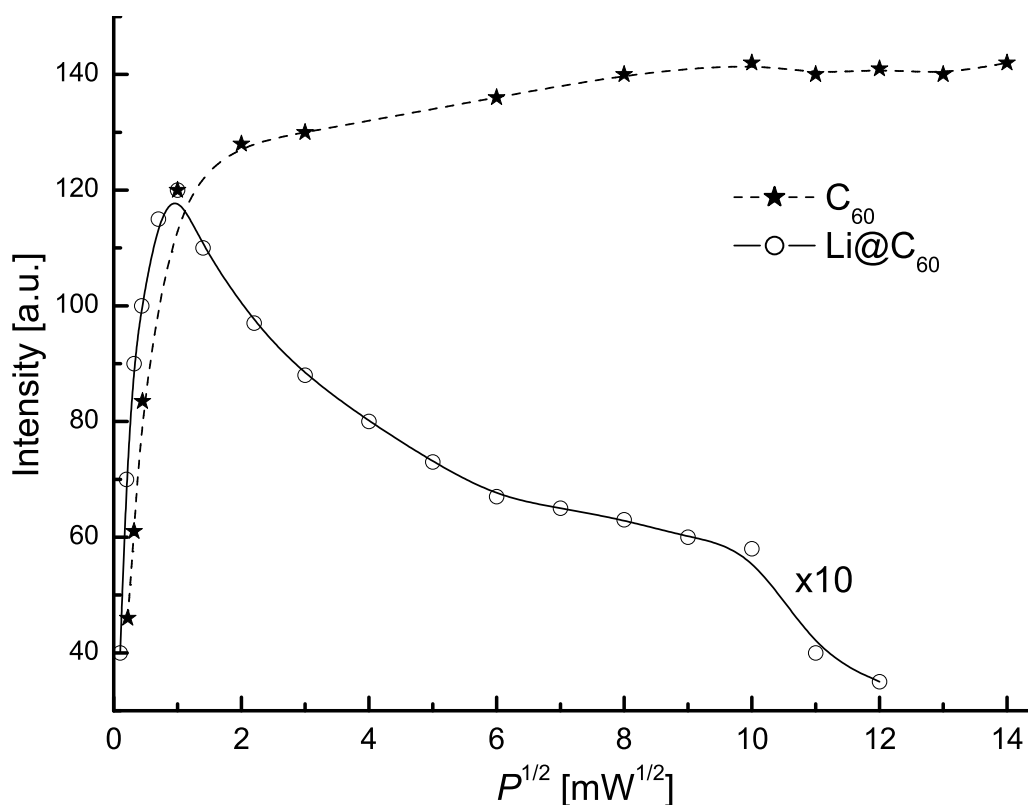


Figure 3.14: EPR signal intensity as a function of the square root of the microwave power for C_{60} and Li@C_{60} measured at room temperature.

signal has been plotted against the square root of the microwave power. In C_{60} the signal keeps increasing as the power is turned up. This is indicative of a system where the spin-lattice relaxation time (T_1) is of the same order of magnitude as the spin-spin relaxation (T_2). These were calculated to be $\sim 10^{-8}$ s. [79]

In the EPR spectra from Li@C_{60} -E2 one single line was present, the hole defect line with $g = 2.0025$, which was also in the pure C_{60} sample. There was no significant difference in the spectra from room temperature measurements and at 77 K, and also no difference between Li@C_{60} in bulk and as a film on a teflon substrate. Compared to C_{60} the line is somewhat broader in the Li@C_{60} spectra, with $\Delta H = 2.5 - 3.1$ G, and the concentration of paramagnetic centres has decreased to $N_{\text{PC}} = 10^{16}/\text{g}$. Upon heating the Li@C_{60} sample to ca 500 °C a new weak EPR line appeared with $g = 2.0004 \pm 0.0005$ (see figure 3.15), also this one present in the C_{60} measurements. The appearance of the C_{60}^- line is accompanied with an increase in the number of PCs to 10^{17} . A possible explanation is that

the heating produces an electron transfer between neighbouring neutral fullerenes creating positively and negatively charged species.

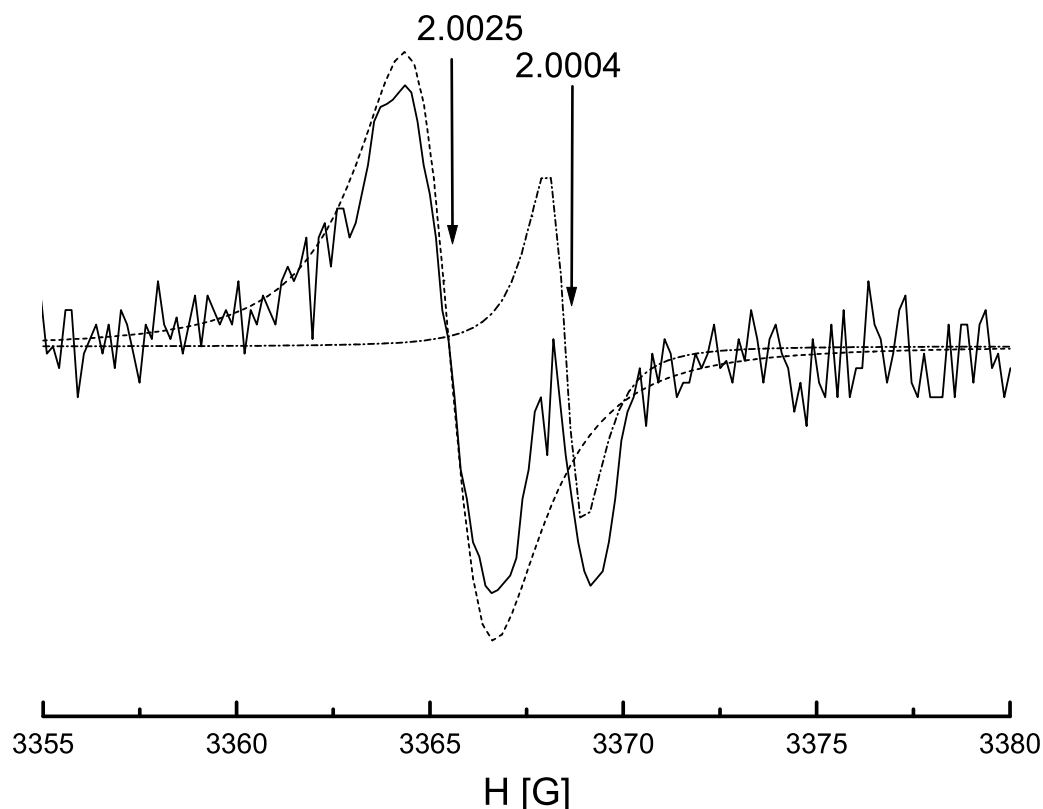


Figure 3.15: ESR spectrum of Li@C₆₀ after heating to ~500°C (full line). Modelling of the lines (dash and dash-dot) gives $g = 2.0025$ and $g = 2.0005$ respectively.

Even if no new EPR lines are found in Li@C₆₀ compared to pure C₆₀ a distinct difference can be found in the dependence of the line intensity on the microwave power (figure 3.14). Where the intensity of the C₆₀ line keeps increasing, the Li@C₆₀ line reaches a maximum at ca 1 mW and then decreases. Calculation of the relaxation times gives $T_1 = 3.2 \cdot 10^{-4}$ s, an increase of four orders of magnitude compared to C₆₀. The spin-spin relaxation time has only increased modestly from $T_2 = 2 \cdot 10^{-8}$ for C₆₀ to $T_2 = 6 \cdot 10^{-8}$ for Li@C₆₀.

The absence of any new lines in the Li@C₆₀ spectrum can be understood in view of the Raman and FTIR measurements discussed in the previous section. Since

Li@C₆₀ exists in the form of dimers or trimers the extra electron forms a double-bond with the electron on the neighbouring molecule, leaving no unpaired electrons to give any EPR signal. The much longer spin-lattice relaxation time can be explained by the lowering of the symmetry due to the binding of the fullerene cages.

3.4 Effect of oxygen on endohedral fullerenes

In this section the effects of air on endohedral fullerenes will be discussed based on LD-TOFMS experiments on La@C₈₂ and conductivity measurements on La@C₈₂ and Li@C₆₀.

3.4.1 LD-TOFMS on films of La@C₈₂ exposed to oxygen

It has been known for a long time that C₆₀ exposed to oxygen deteriorates slowly over time, and that the process goes faster if the fullerenes are exposed to UV light [80] or high temperatures [81]. Endohedral fullerenes have also been investigated for oxygen sensitivity using MS. Callahan *et al.* found that the amount of La@C_n (n=60–82) in fullerene soot decreased as the soot was exposed to air [82]. Similarly, also in fullerene soot, Hettich and co-workers saw the release of Sr from Sr@C₆₀ after several weeks of air exposure, evidenced by the appearance of previously nonexistent peaks from Sr⁺, SrO⁺, SrCO₃⁺, Sr₂O₂⁺ and Sr₂CO₂⁺ in their LD mass spectra [83].

In order to perform a more quantitative analysis of the effect of oxygen on metallofullerenes we prepared thin (500–1000 Å) films of La@C₈₂ by evaporating HPLC purified material from a quartz ampoule onto substrates of glass or aluminium. The evaporation was performed in a vacuum chamber with a base pressure of 10⁻⁷ mbar. The films were quickly transferred to the TOF-MS, exposing them only briefly to atmospheric oxygen (<5 min). To expose the fullerenes to oxygen the films were taken out of the mass spectrometer and stored in ambient air in the laboratory.

LD-TOFMS, with a laser fluence of ~18 mJ/cm², on freshly deposited films of La@C₈₂ shows the characteristic shrink-wrapping of the enclosed metal atom from sequential loss of C₂-units, but no or only very small amounts of lanthanum or smaller carbon fragments. This can be seen in the top frame of figure 3.16.

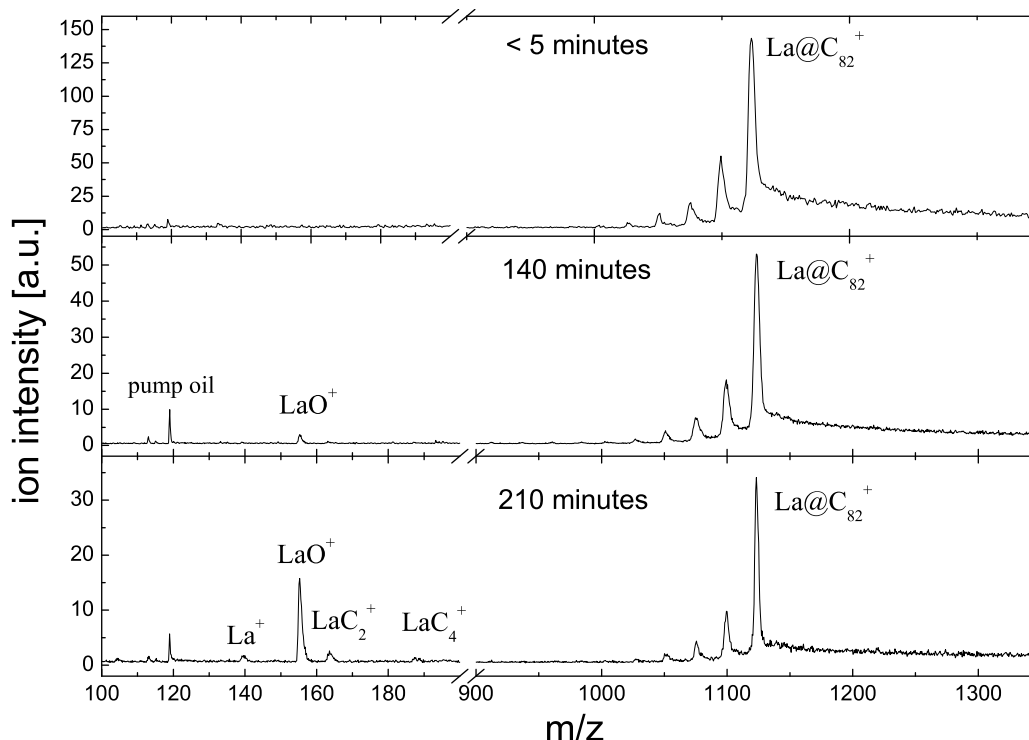


Figure 3.16: Positive mode LD-TOF mass spectra of a film of La@C_{82} after various times of exposure to air.

La-carbide fragments are found in LD-TOFMS experiments with higher laser fluence and come from complete destruction of the metallofullerene and loss of the fullerene structure [37]. However, after only a few hours exposure to air first LaO^+ and then LaC_n^+ ($n = 0, 2, 4$) appears in the mass spectra. This is accompanied with a decrease of the La@C_{82}^+ signal. It is notable, however, that the relative intensities of the peaks in the fragmentation pattern remain unchanged, as expected for spectra taken at the same laser fluence. After roughly one month storage of the film in ambient laboratory air the mass spectrum in figure 3.17 was taken. It shows a very large LaO^+ peak, but also oxidised metallofullerene ions. $\text{La@C}_{76}\text{O}^+$ and $\text{La@C}_{82}\text{O}^+$ are clearly visible, but $\text{La@C}_{78}\text{O}^+$ and $\text{La@C}_{80}\text{O}^+$ may be hinted at as shoulders on the La@C_{80}^+ and La@C_{82}^+ peaks respectively. Another new feature not seen in the pristine films is the presence of empty C_{82-n}^+ .

Experiments were also performed using negative ion LD-TOFMS, shown in figure 3.18. In the case of pristine metallofullerene films the La@C_{82}^- is the dominating peak, with a tiny $\text{La@C}_{82}\text{O}^-$ as only companion. No fragmentation is detected

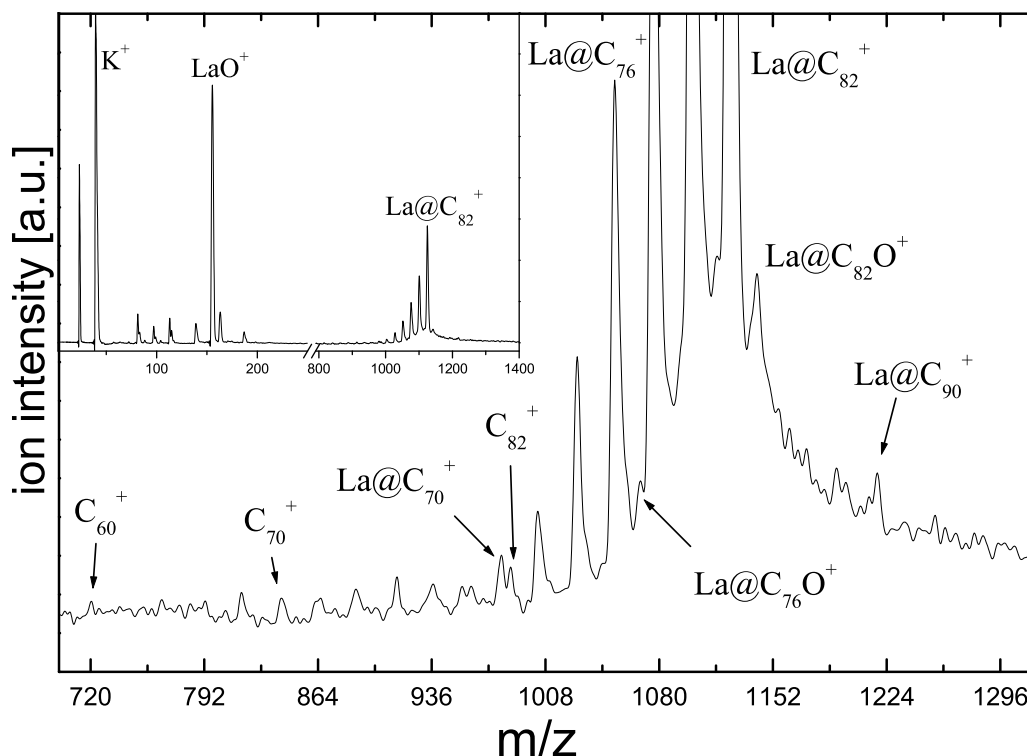


Figure 3.17: LD-TOFMS of a thin La@C₈₂ film exposed to air for 35 days. The inset shows the lower and the higher mass region with fragmentation and a prominent peak from LaO⁺. The close-up of the higher mass region reveal the presence of oxygenated species.

despite a laser fluence of 15 mJ/cm². This is not surprising, however, and is also observed in negative mode MS of C₆₀. The electron affinities of C₆₀ and La@C₈₂ are much lower than the dissociation energy for C₂ loss, making loss of the extra electron the vastly dominating fragmentation channel for negatively charged (metallo)fullerenes. However, after a few hours in air small carbon clusters appear in the mass spectra, as well as both La@C₈₀⁻ and empty C₈₂⁻. The amount of these increase over time. In the bottom frame of figure 3.18 we can also find doubly oxidised La@C₈₀O₂⁻. An unidentified peak at ~1159 u is marked with an asterisk. It may be the result of a chlorine attached to the La@C₈₂. The mass of this should be 1158 u for ³⁵Cl.

It seems clear that oxygen, most likely from O₂ in the air, reacts with the metallofullerenes and increases the likelihood for loss of the internal lanthanum atom. It has been suggested [84] in the case of C₆₀ that O₂ molecules can react with

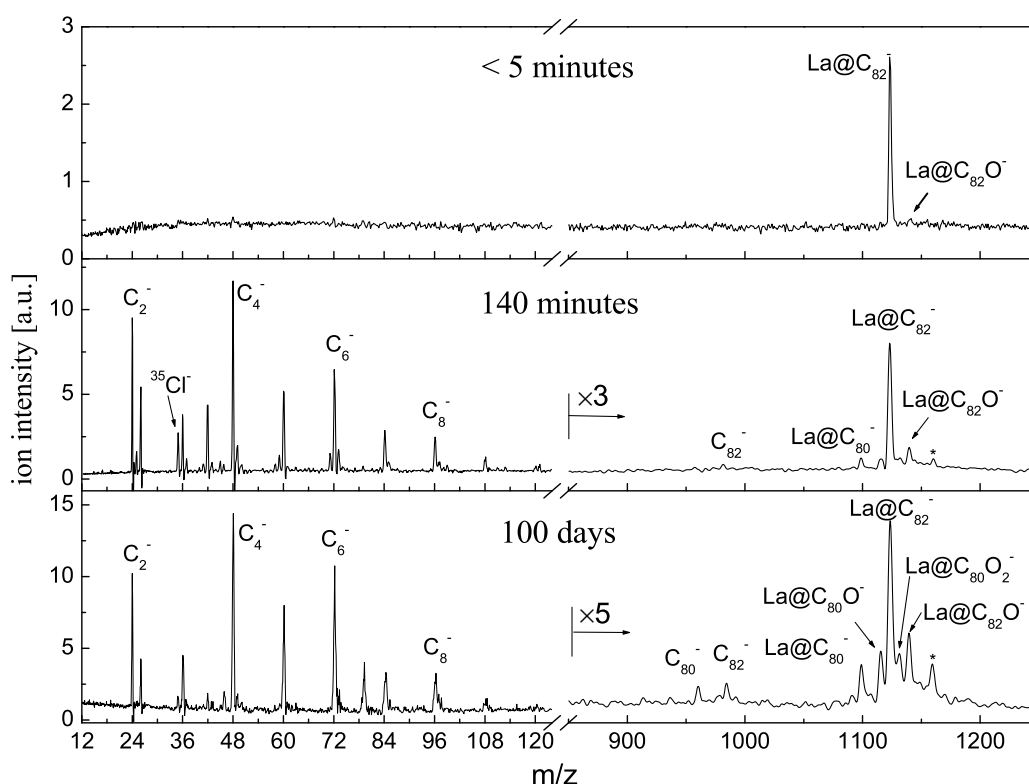


Figure 3.18: Negative mode LD-TOF mass spectra of a film of La@C_{82} after various times of exposure to air.

a double bond in the fullerene cage. The process involves energy transfer from the excited triplet state in the C_{60} to the oxygen molecule and results in a severed $\text{C}=\text{C}$ bond that leaves the cage open, with $\text{C}=\text{O}$ groups on each side of the gap. The damaged C_{60}O_2 can fragment by the loss of CO , CO_2 or 2CO . CO and CO_2 has been observed in photoemission studies of solid O_2 in contact with C_{60} [85], and the products C_{59}O^- and C_{59}^- in collision-induced dissociation of C_{60}O^- and $\text{C}_{60}\text{O}_2^-$ [82]. Small negatively charged carbon clusters have been observed earlier in reactions between laser ablated hot (empty) fullerenes and molecular oxygen clusters [86]. These probably originate from the fragmentation of unstable products like the C_{59} .

In figure 3.19 the ratio of LaO^+ and LaC_n^+ fragments to La@C_{82}^+ is compared for film exposed to oxygen for different periods of time. Since the only source of La is from the metallofullerenes the aforementioned fragments are obviously products of the destruction of the endohedral fullerene. It is known that oxygen diffuses into C_{60} films, causing great changes to the conductivity of the film [87]. The

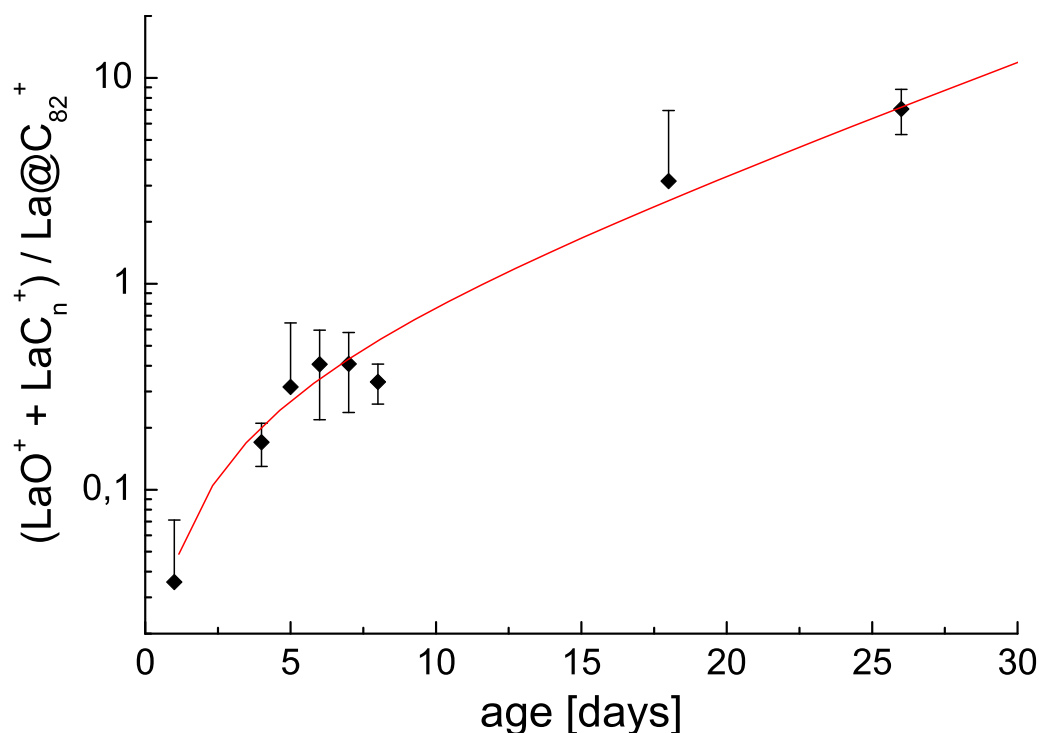


Figure 3.19: The ratio $(\text{LaO}^+ + \text{LaC}_n^+) / \text{La@C}_{82}^+$ measured from positive mode LD-TOFMS spectra of films of La@C_{82} exposed to oxygen for varying periods of time.

concentration of oxygen in the film grows roughly exponentially, with a typical time constant of days [87]. Assuming that the La@C_{82} decays exponentially, as a consequence of the increased amount of oxygen in the film, this will give the ratio of fragments to intact fullerenes as

$$R(t) = \sigma (e^{kt} - 1), \quad (3.2)$$

where k is the rate constant for the destruction of the metallofullerenes and σ is a factor related to difference in detection efficiency and ionisation potential between the parent and the daughter molecules. Fitting the data in figure 3.19 with this function gives $k = (1.2 \pm 0.5) \cdot 10^{-6} \text{ s}^{-1}$, which corresponds to a half-life of 6.6 days, and $\sigma = 0.54 \pm 0.12$. The latter corresponds reasonably to the detection efficiency correction factor between La@C_{82} and the fragments [37].

The effects of oxygen on fragmentation of C_{60} , described in articles mentioned above, were investigated on fullerene-oxides prepared in manners differing from our experiments. C_{60} is reasonably stable in air and films of C_{60} exposed to am-

bient atmosphere do not show any oxygenated species in LD-TOFMS measurements. However, La@C₈₂ has a higher electron affinity than C₆₀ [88], and is more likely to react strongly with oxygen. There is thus reason to believe that atmospheric oxygen can affect La@C₈₂ also without for example photoexcitation. If O₂ molecules are indeed able to break open the fullerene cage also in La@C₈₂, that could serve as explanation for the increased propensity for loss of the encapsulated lanthanum atom. The La@C₈₂O_n⁻ ($n = 0, 1, 2$) seen in the mass spectra is likely to be due to loss of C₂, CO and CO₂ from La@C₈₂O₂, mirroring the reaction found for C₆₀. Also, the presence of the empty fullerene anions C_{82-2n}⁻ is probably not due to sequential C₂ loss, due to the low probability of that reaction channel compared to loss of the electron, but direct fragmentation of oxygenated La@C₈₂. We do not detect any unevenly numbered fullerenes like La_m@C₈₁ ($m = 0, 1$) in our mass spectra similar to what was found for C₆₀, and it is likely that if they are formed they readily fragment into smaller pieces, perhaps completely breaking up the fullerene structure. The many small carbon fragments and La-carbides found can be indicative of this.

It is obvious that oxygen in the air has an effect on the stability of the La@C₈₂ in thin films, and increases the tendency for fragmentation and loss of the internal atom in LD-TOFMS experiments.

3.4.2 Conductivity of thin endohedral fullerene films and the effects of oxygen exposure

Measurements of the conductivity of C₆₀ have been made many times over the years, and it is known that the conductivity is lowered by several order of magnitude by the presence of oxygen in the sample [89]. The same is true for higher fullerenes (C₇₆, C₇₈, and C₈₄) according to a recent study [90].

We have performed measurements on the endohedral fullerenes Li@C₆₀ and La@C₈₂, and for comparative reasons on the empty C₆₀.

In figure 3.20 the result of I-V measurements on C₆₀ are shown. The measurements were performed after different deposition times, i.e. with differently thick fullerene films. The final thickness of the film, after 11 minutes deposition, was measured by profilometer to be ~800 nm. Each measurement was performed in two directions, with increasing and decreasing voltage. The hysteresis-like behaviour is likely due to charging effects of the sample during measurements, and is pronounced at very low currents, but disappears at higher current levels. The conductivity is determined by fitting a straight line through the origin, as shown

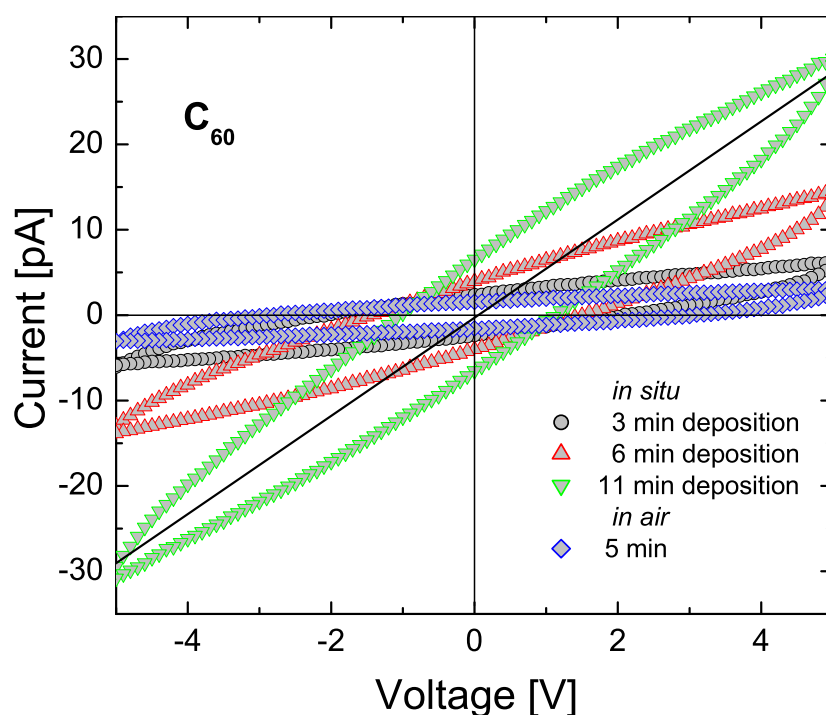


Figure 3.20: I-V measurement on a thin film of C_{60} after different deposition times and after ~ 5 min exposure to air.

for one of the curves in figure 3.20. For C_{60} the resistivity was measured to be $52 \text{ M}\Omega \text{ cm}$, which is in good agreement with results found in the literature [91,92]. The measurements performed after the fullerenes were exposed to air for five minutes show an increase in the resistivity of about one order of magnitude. This is in line with expectations [89]. The measurements on $\text{Li}@C_{60}$ were performed using purified material from the E2 fraction. As was shown in previous sections $\text{Li}@C_{60}$ exists as a trimer. It is thought that the weak intercage bonds are broken upon heating and the fullerenes are deposited as monomers, but it is likely that they oligomerise again on the surface, but not necessarily in the same form. For the resistivity of $\text{Li}@C_{60}$ we measured a value of $1.5 \text{ k}\Omega \text{ cm}$ for a freshly deposited 30 nm thick film (figure 3.21, top frame). This is more than four orders of magnitude lower than the value for C_{60} . But, as can be seen in figure 3.21b, only a very brief exposure to oxygen, in this case only two minutes, leads to a dramatic increase of the resistivity. After another hour of air exposure the conductivity has dropped to levels comparable to empty C_{60} .

Recent STS-investigations of $\text{La}@C_{82}$ show that it has a metallic electronic structure [63], and can be expected to be a good conductor. The transport measure-

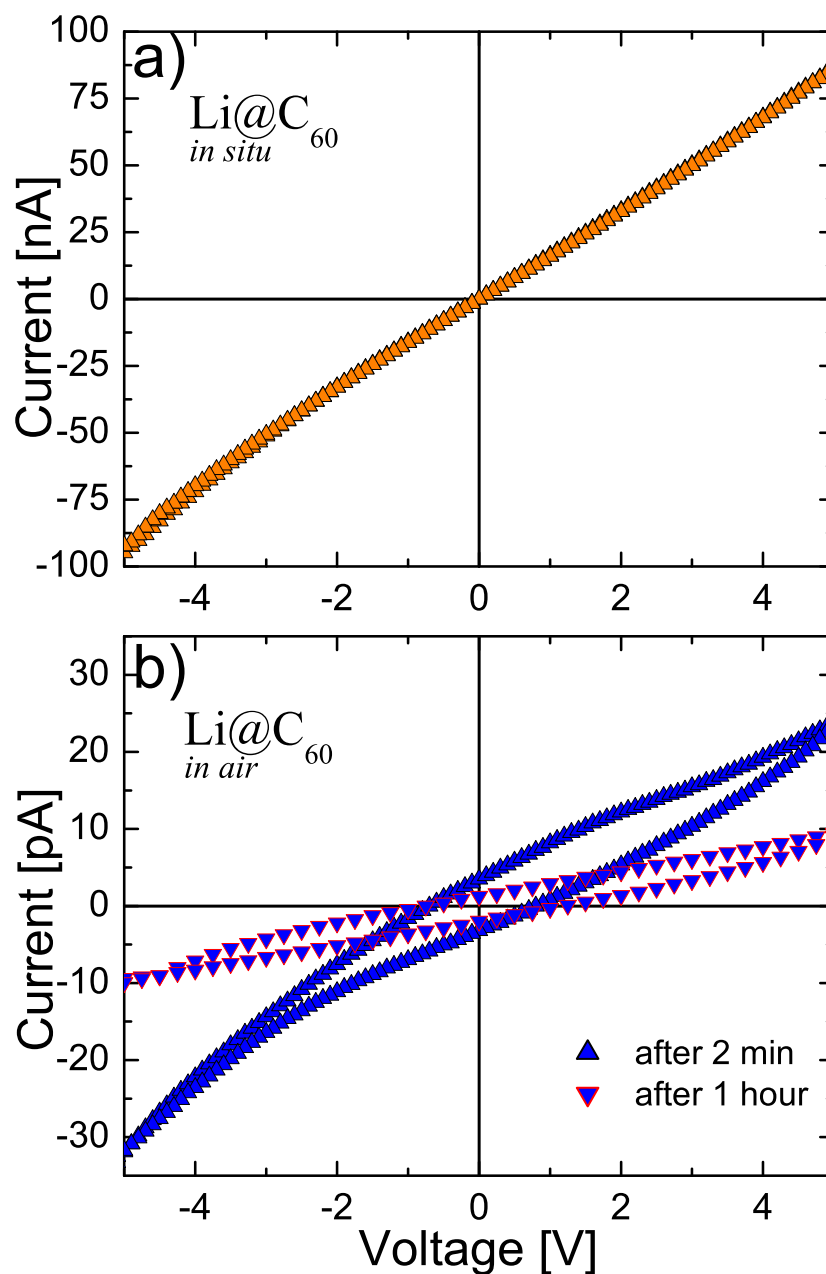


Figure 3.21: I-V measurement on a thin film of Li@C_{60} . The upper graph shows the I-V characteristics of a freshly deposited film, while the lower graphs display the result after different times of exposure to air. Note the change in scale of the ordinate.

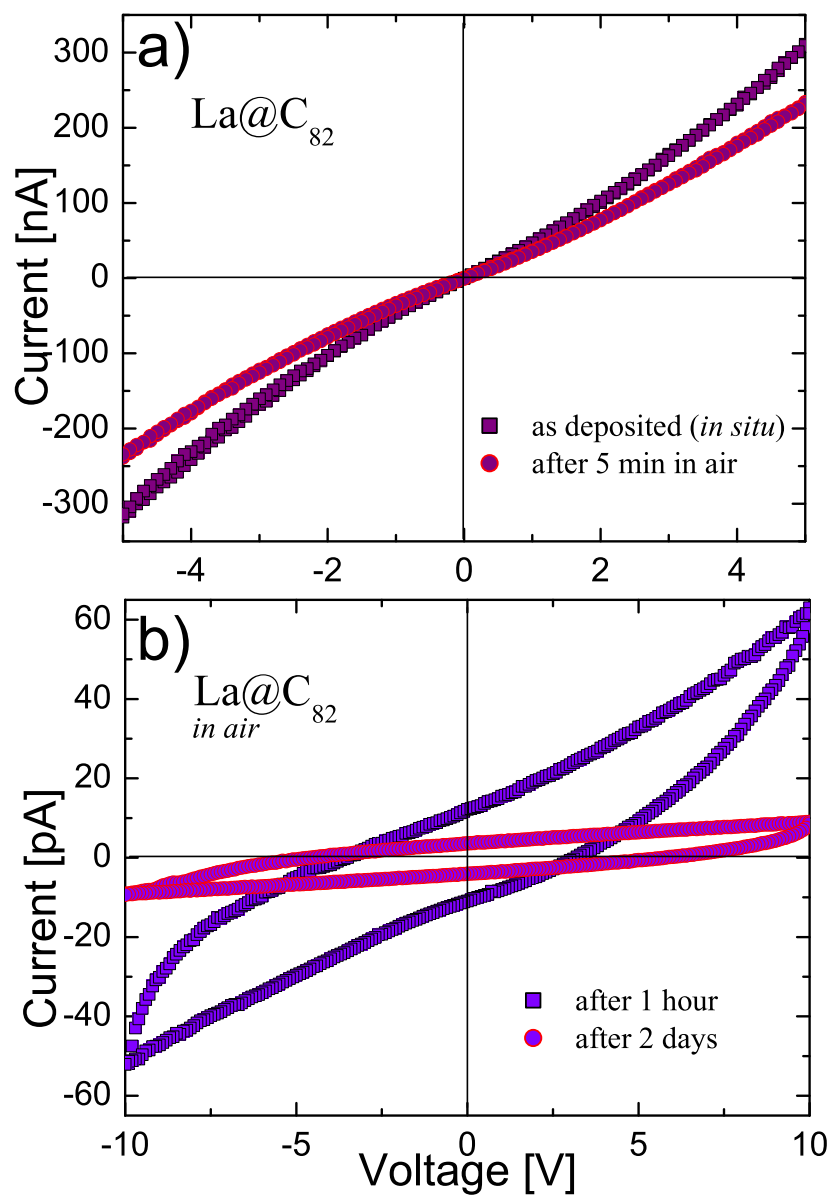


Figure 3.22: I-V measurement on a thin film of Li@C_{60} . The upper graph shows the I-V characteristics of a freshly deposited film and after five minutes of air exposure, while the lower graphs display the result after some longer periods in air.

ments on freshly deposited films (figure 3.22a) gives a resistivity for LaC₈₂ of 300 Ω cm. Also for LaC₈₂ we notice a decrease in conductivity, however much slower than for Li@C₆₀. After five minutes in air the resistivity has increased by 25%, and only after days of exposure does the conductivity approach the levels of C₆₀, as can be seen in figure 3.22b.

We saw in section 3.4.1 that La@C₈₂ is affected by oxygen, and that the effects start becoming visible in LD-TOFMS after about two hours of exposure to air. However, the conductivity is affected noticeably after a much shorter time, and for Li@C₆₀ there is a dramatic change in conductivity after only brief exposure. Oxygen influences the conductivity of C₆₀ as well. Immediately upon exposure, oxygen starts diffusing into the intergrain boundaries of a fullerene film [87]. This is a process that takes several minutes, and can lower the conductivity in C₆₀ by an order of magnitude or two by quenching the electronic transport. Over several hours or days the oxygen continues to diffuse into the interstitial places of the fullerene grains. Presumably a similar behaviour is found for the metallofullerenes. One can also see a clear difference in the I-V characteristics between Li@C₆₀ and La@C₈₂, where the former shows a clearly ohmic dependence, and the latter has a non-linear behaviour. To explain this behavior we need to find the conduction mechanism.

Some preliminary measurements have been performed on the temperature dependent conductivity of C₆₀. These are to be followed by similar experiments for La@C₈₂. During the measurements, a fullerene film was deposited, as described above, after which the temperature of the sample was increased slowly by an electric heater. Transport measurements were performed at intervals of 5 or 10 degrees. When the sample reached the desired temperature the heating current was turned off and the sample was left to cool down in vacuum, while the measurement were repeated for the decreasing temperature cycle. The temperature dependence of the resistance of a fullerene film, measured *in situ*, is plotted in figure 3.23. The resistance is plotted on a log scale against 1000/T on an Arrhenius plot. During increasing of T, the resistivity shows a linear behaviour in the Arrhenius plot. This is the normal case of a semiconductor, with an activated conductance $\sigma \propto e^{-E_a/k_B T}$, where E_a is the activation energy. However, at a temperature of ca 110 °C the behaviour changes, and around 150 °C the resistivity stops decreasing. During the decrease of the temperature the behaviour of the resistance in the Arrhenius plot is clearly not linear. Some change in the conduction mechanism occurs, but the details are not yet known. However, a hint can be found by looking at the structure of the fullerene film in AFM before and after heating, as seen in figure 3.24. A clear difference between the two images can be seen, were the upper picture, taken on a freshly deposited film, has much finer

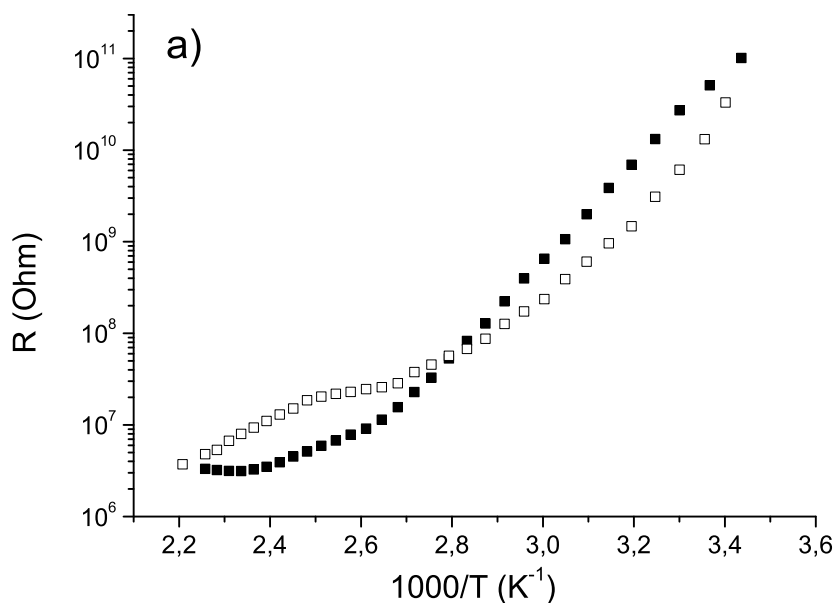


Figure 3.23: Temperature dependence of the resistance of a fullerene film. The logarithm of the resistance is plotted against the inverse of the temperature in an Arrhenius plot. The full squares are for increasing temperature, and the empty squares for decreasing T .

grain than the film after heating to 180 °C, shown in the lower image. This change of structure probably affects the conductivity, but further experiments are needed to provide a conclusive answer. Notable is also that the change in conductivity and structure has not been reported in earlier measurement on fullerene films, see e.g. [87].

We also exposed a C_{60} film to air for 15 minutes, which lowered the conductivity by about 1 order of magnitude. After annealing for ca 20 hours at 150 °C the conductivity returned to its original value. This is in line with earlier observations [87].

Experiments on the temperature dependent conductivity of metallofullerenes are underway. Particularly interesting is the annealing experiment, that might reveal whether the effect of oxygen exposure is reversible, as for C_{60} , or if the damage is permanent as might be suggested by the LD measurements.

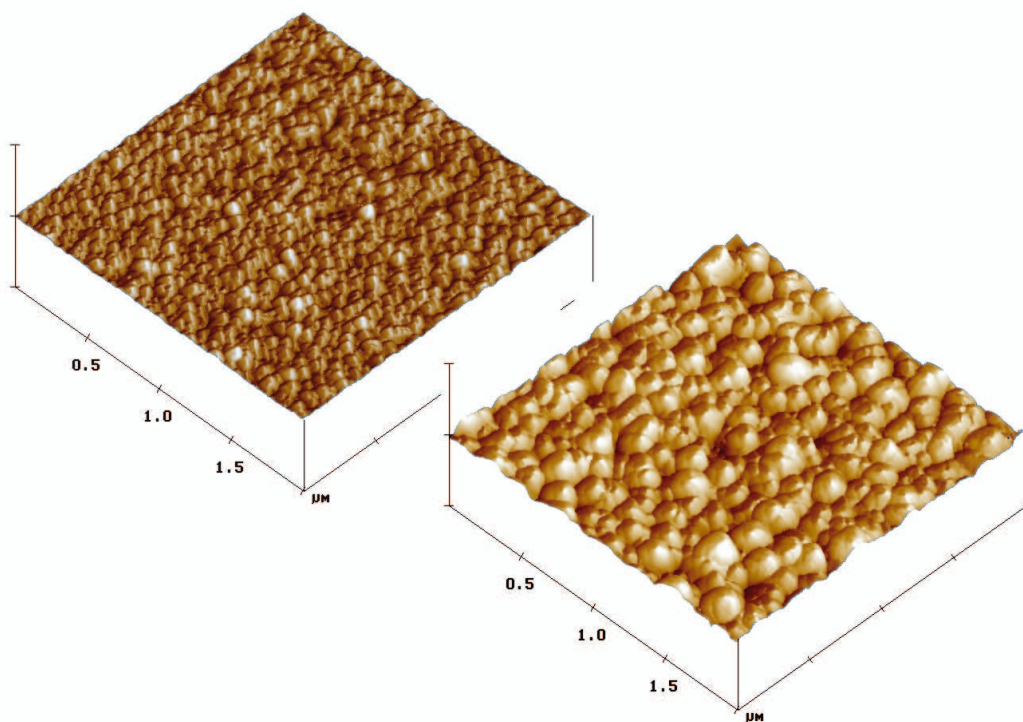


Figure 3.24: AFM images of the fullerene film. The upper image shows the film directly after deposition, and the lower image is taken after heating the sample to 180 °C.

4

Conclusions and Outlook

“Would you tell me, please, which way I ought to go from here?”

“That depends a good deal on where you want to get to,” said the Cat.

“I don’t much care where—,” said Alice

“Then it doesn’t matter which way you go,” said the Cat.

“—so long as I get *somewhere*,” Alice added as an explanation.

“Oh, you’re sure to do that”, said the Cat, “if you only walk long enough.”

In this thesis recent investigations concerning production, structure, and stability of the endohedral fullerenes $\text{Li@C}_{60/70}$ and La@C_{82} have been presented. A brief description was given of a new surface ionisation source that was designed to cut the costs of using expensive ion emitters, and enable the production of non-alkali metallofullerenes. This is the scope of ongoing experiments.

The produced $\text{Li@C}_{60/70}$ was investigated using LD-TOFMS, EPR, and vibrational spectroscopy to determine the structure of the metallofullerenes. It could be concluded that the two fractions of Li@C_{60} found in HPLC purification of the ion bombarded fullerenes are dimers and trimers of Li@C_{60} . EPS investigation showed no new resonances in Li@C_{60} compared to pristine C_{60} , something that can be explained by the formation of double-bonded dimers and trimers, pairing the electrons donated to the carbon cage by the internal atom. The EPR signal did show a difference in the dependence on microwave power between empty and filled C_{60} .

LD-TOFMS investigation of thin films of La@C_{82} showed that the fullerenes reacted with oxygen in the air. The oxygen increased the inclination of loss of the internal La atom compared to films not exposed to air, that show fragmentation mostly through C_2 loss, so called “shrink-wrapping”. An explanation could be an oxygen-reaction opening the cage, allowing the La to slip out more easily than in intact molecules.

Transport measurements of the metallofullerenes Li@C_{60} and La@C_{82} show that their conductivity is much higher than that of C_{60} , but the measurements also confirm the films’ oxygen sensitivity. Upon exposure to air the conductivity rapidly drops, and after prolonged exposure reaches that of pristine C_{60} .

Acknowledgements

On this page, usually one of the first, and in many cases only, read in a thesis, I would like to thank Professor Eleanor Campbell for giving me the opportunity to work in her group. She is an invaluable source of the inspiration, information, and sometimes intimidation, needed to get the work done. I am also grateful for the support of our chemist Dr. Andrei Gromov, who has guided me through the magic of chemistry. Dr. Vladimir Popok did a great job during the work with the transport measurements. Thanks also to Dr. Andreas Lassesson, newly-fledged Kiwi, my predecessor in the endo-research, who taught me all about lab-work, and together with whom many of the experiments were performed.

Life in the lab and office would be much more difficult if not for Mats taking care of things. Sometimes a car-mechanic turned engineer is just what you need. Wiman and the other guys in the physics work-shop have always been helpful in trying to interpret my sometimes less than perfect drawings, and build me the strange stuff I needed.

Thanks Heini for keeping us alive!

The Martins, Raluca, Emma, Dag, and all the other people in the Atomic Physics group: You are great work-mates and lots of fun to be around.

Finally I would like to extend my gratitude to my family and friends for their love and support, and for retaining my sanity. . . Cheers!

Bibliography

- [1] Lee, S. T. and Lifshitz, Y., “Materials science: The road to diamond wafers,” *Nature*, Vol. 424, 2003, 500–501.
- [2] Rohlfing, E. A., Cox, D. M., and Kaldor, A., “Production and characterization of supersonic carbon cluster beams,” *J. Chem. Phys.*, Vol. 81, No. 7, 1984, 3322–3330.
- [3] Kroto, H. W., Heath, J. R., O’Brien, S. C., Curl, R. F., and Smalley, R. E., “C₆₀ : Buckminsterfullerene,” *Nature*, Vol. 318, 1985, 162–163.
- [4] “The Nobel e-Museum,”
<http://nobelprize.org/chemistry/laureates/1996/>, Accessed 2004-11-05.
- [5] Krätschmer, W., Lamb, L. D., Fostiropoulos, K., and Huffman, D. R., “Solid C₆₀ : a new form of carbon,” *Nature*, Vol. 347, 1990, 354.
- [6] Dresselhaus, M. S., Dresselhaus, G., and Eklund, P. C., *Science of fullerenes and carbon nanotubes*, Academic Press, San Diego, 1996.
- [7] Thoreau, H. D., *Walden, or, life in the woods*, Boston, 1854.
- [8] Lifshitz, C., “Carbon clusters,” *Int. J. Mass Spectrom.*, Vol. 200, No. 1-3, 2000, 423–442.

- [9] Campbell, E. E. B., "Fullerenes," *Europhys. News*, Vol. 33, No. 6, 2002, 202–204.
- [10] Heath, J. R., O'Brien, S. C., Zhang, Q., Liu, Y., Curl, R. F., Tittel, F. K., and Smalley, R. E., "Lanthanum complexes of spheroidal carbon shells," *J. Am. Chem. Soc.*, Vol. 107, No. 25, 1985, 7779–7780.
- [11] Mikawa, M., Kato, H., Okumura, M., Narazaki, M., Kanazawa, Y., Miwa, N., and Shinohara, H., "Paramagnetic Water-Soluble Metallofullerenes Having the Highest Relaxivity for MRI Contrast Agents," *Bioconjugate Chem.*, Vol. 12, 2001, 510–514.
- [12] Bolskar, R. D., Benedetto, A. F., Husebo, L. O., Price, R. E., Jackson, E. F., Wallace, S., Wilson, L. J., and Alford, J. M., "First Soluble M@C₆₀ Derivatives Provide Enhanced Access to Metallofullerenes and Permit in Vivo Evaluation of Gd@C₆₀[C(COOH)₂]₁₀ as a MRI Contrast Agent," *J. Am. Chem. Soc.*, Vol. 125, No. 18, 2003, 5471–5478.
- [13] Shinohara, H., "Endohedral metallofullerenes," *Rep. Prog. Phys.*, Vol. 63, 2000, 843–892.
- [14] Ohtsuki, T., Yuki, H., Muto, M., Kasagi, J., and Ohno, K., "Enhanced Electron-Capture Decay of ⁷Be Encapsulated in C₆₀ Cages," *Phys. Rev. Lett.*, Vol. 93, No. 11, 2004, 112501.
- [15] Chai, Y., Guo, T., Jin, C., Haufler, R. E., Felipe Chibante, L. P., Fure, J., Wang, L., Alford, J. M., and Smalley, R. E., "Fullerenes with Metals Inside," *J. Phys. Chem.*, Vol. 95, 1991, 7564–7568.
- [16] Shinohara, H., Sato, H., and Saito, Y., "Mass Spectroscopic and ESR Characterization of Soluble Yttrium-Containing Metallofullerenes YC₈₂ and Y₂C₈₂," *J. Phys. Chem.*, Vol. 96, 1992, 3571–3573.
- [17] Mowrey, R. C., Ross, M. M., and Callahan, J. H., "Molecular Dynamics Simulations and Experimental Studies of the Formation of Endohedral Complexes of Buckminsterfullerene," *J. Phys. Chem.*, Vol. 96, 1992, 4755–4761.
- [18] Christian, J. F., Wan, Z., and Anderson, S. L., "Ne⁺+C₆₀ collisions: The dynamics of charge and energy transfer, fragmentation, and endohedral complex formation," *J. Chem. Phys.*, Vol. 99, 1993, 3468–3479.
- [19] Murry, R. L. and Scuseria, G. E., "Theoretical Evidence for a C₆₀ "Window" mechanism," *Science*, Vol. 263, 1994, 791–793.

- [20] Saunders, M., Jiménez-Vázquez, H. A., Cross, R. J., Mroczkowski, S., Gross, M. L., Giblin, D. E., and Poreda, R. J., "Incorporation of Helium, Neon, Argon, Krypton, and Xenon into Fullerenes using High Pressure," *J. Am. Chem. Soc.*, Vol. 116, 1994, 2193–2194.
- [21] Hirata, T., Hatakeyama, R., Mieno, T., and Sato, N., "Production and Control of K-C₆₀ plasma for material processing," *J. Vac. Sci. Technol. A*, Vol. 14, No. 2, 1995, 615–618.
- [22] Hirata, I., Otomo, Y., and Hatakeyama, R., "Production and control of La plasma and application to fullerene-related material process," *Thin Solid Films*, Vol. 407, No. 1-2, 2002, 32–7.
- [23] Neeb, M., Klingeler, R., Bechthold, P. S., Kann, G., Wirth, I., Eisebitt, S., and Eberhardt, W., "Deposition of endohedral fullerenes from a laser evaporation cluster source," *Appl. Phys. A*, Vol. 72, No. 3, 2001, 289–93.
- [24] Klingeler, R., Bechthold, P. S., Neeb, M., and Eberhardt, W., "An experimental setup for nondestructive deposition of size-selected clusters," *Rev. Sci. Instrum.*, Vol. 73, No. 4, 2002, 1803–1808.
- [25] Wan, Z., Christian, J. F., Basir, Y., and Anderson, S. L., "Collision of alkali ions with C₆₀/C₇₀: Insertion, thermionic emission, and fragmentation," *J. Chem. Phys.*, Vol. 99, No. 8, 1993, 5858–5870.
- [26] Campbell, E. E. B., Ehlich, R., Hielscher, A., Frazao, J. M. A., and Hertel, I. V., "Collision energy dependence of He and Ne capture by C₆₀⁺," *Z. Phys. D*, Vol. 23, No. 1, 1992, 1–2.
- [27] Tellgmann, R., Krawez, N., Lin, S. H., Hertel, I. V., and Campbell, E. E. B., "Endohedral fullerene production," *Nature*, Vol. 382, 1996, 407–408.
- [28] Heinz, O. and Reaves, R. T., "Lithium Ion Emitter for Low Energy Beam Experiments," *Rev. Sci. Instrum.*, Vol. 39, No. 8, 1968.
- [29] Campbell, E. E. B., Tellgmann, R., Krawez, N., and Hertel, I. V., "Production and LDMS characterisation of endohedral alkali-fullerene films," *J. Phys. Chem. Solids*, Vol. 58, No. 11, 1997, 1763–1769.
- [30] Gromov, A., Krätschmer, W., Tellgmann, R., and Campbell, E. E. B., "Extraction and HPLC purification of Li@C_{60/70}," *Chem. Commun.*, 1997, 2003–2004.

- [31] Lassesson, A., *Fullerenes with confined atoms : the structure and dynamics of Li@C₆₀ and La@C₈₂*, Ph. D. thesis, Chalmers University of Technology and Göteborg University, 2003.
- [32] Wolf, B., *Handbook of ion sources*, CRC Press, Boca Raton, 1995.
- [33] Rasser, B. and Remy, M., “Experiments on a new surface ionization source with Lithium,” *Rev. Sci. Instr.*, Vol. 46, No. 3, 1975, 325–326.
- [34] Rasser, B., Pearson, D. I. C., and Remy, M., “Surface ionization for heavy ions,” *Rev. Sci. Instr.*, Vol. 51, No. 4, 1980, 474–477.
- [35] Naaman, R. and Vager, Z., “An electron multiplier capable of working at low vacuum: The microsphere plate,” *Rev. Sci. Instrum.*, Vol. 67, No. 9, 1996, 3332–3333.
- [36] Campbell, E. E. B., Ulmer, G., Hasselberger, B., Busmann, H.-G., and Hertel, I. V., “An intense, simple carbon cluster source,” *J. Chem. Phys.*, Vol. 93, No. 9, 1990, 6900–6907.
- [37] Lassesson, A., Gromov, A., Mehlig, K., Taninaka, A., Shinohara, H., and Campbell, E. E. B., “Formation of small lanthanum-carbide ions from laser induced fragmentation of La@C₈₂,” *J. Chem. Phys.*, Vol. 119, 2003, 5591.
- [38] Winter, B., Mitzner, R., Kusch, C., Campbell, E. E. B., and Hertel, I. V., “On the mechanism of C₆₀ thin film laser-induced desorption,” *J. Chem. Phys.*, Vol. 104, No. 22, 1996, 9179–9190.
- [39] Wiley, W. C. and McLaren, I. H., “Time-of-Flight Mass Spectrometer with Improved Resolution,” *Rev. Sci. Instr.*, Vol. 26, No. 12, 1955, 1150–1157.
- [40] Lassesson, A., Mehlig, K., Gromov, A., Taninaka, A., Shinohara, H., and Campbell, E. E. B., “The fragmentation and ionization of highly excited La@C₈₂,” *J. Chem. Phys.*, Vol. 117, No. 21, 2002, 9811–9817.
- [41] Lebedkin, S., Gromov, A., Giesa, S., Gleiter, R., Renker, B., Reitschel, H., and Krätschmer, W., “Raman scattering study of C₁₂₀, a C₆₀ dimer,” *Chem. Phys. Lett.*, Vol. 285, 1998, 210–215.
- [42] Weisstein, E. W., “‘Crystallographic Point Groups.’ From MathWorld—A Wolfram Web Resource.” <http://mathworld.wolfram.com/CrystallographicPointGroups.html>, Accessed 2003-03-21.

- [43] Harris, D. C. and Bertolucci, M. D., *Symmetry and spectroscopy : an introduction to vibrational and electronic spectroscopy*, Oxford University Press, New York, 1978.
- [44] von Helden, G., Holleman, I., Meijer, G., and Sartakow, B., "Excitation of C_{60} with chirped free electron laser," *Opt. Express*, Vol. 4, No. 2, 1999, 46–52.
- [45] Campbell, E. E. B., Fanti, M., Hertel, I. V., Mitzner, R., and Zerbetto, F., "The hyperpolarisability of an endohedral fullerene: $Li@C_{60}$," *Chem. Phys. Lett.*, Vol. 288, No. 1, 1998, 131–7.
- [46] Bernshtein, V. and Oref, I., "Surface migration of endohedral Li^+ on the inner wall of C_{60} ," *Phys. Rev. A*, Vol. 62, 2000, 033201.
- [47] Dunlap, B. I., Ballester, J. L., and Schmidt, P. P., "Interactions between C_{60} and Endohedral Alkali Atoms," *J. Phys. Chem.*, Vol. 96, No. 9781-9787, 1992, Calculation of the Li potential energy surface in C_{60} .
- [48] Delaney, P. and Greer, J. C., " C_{60} as a Faraday cage," *Appl. Phys. Lett.*, Vol. 84, No. 3, 2004, 431–433.
- [49] Joslin, C. G., Yang, J., Gray, C. G., Goldman, S., and Poll, J. D., "Infrared rotation and vibration—rotation bands of endohedral fullerene complexes. Absorption spectrum of $Li^+@C_{60}$ in the range 1–1000 cm^{-1} ," *Chem. Phys. Lett.*, Vol. 208, 1993, 86–92, Calculations of absorption spectra.
- [50] Davydov, V. A., Kashevarova, L. S., Rakhmanina, A. V., Senyavin, V. M., Ceolin, R., Szwarc, H., Allouchi, H., and Agafonov, V., "Spectroscopic study of pressure-polymerized phases of C_{60} ," *Phys. Rev. B*, Vol. 61, 2000, 11936–11945.
- [51] Gromov, A., Krawez, N., Lassesson, A., Ostrovskii, D. I., and Campbell, E. E. B., "Optical properties of endohedral $Li@C_{60}$," *Curr. Appl. Phys.*, Vol. 2, No. 1, 2002, 51–55.
- [52] Dresselhaus, M. S., Dresselhaus, G., and Saito, R., "Carbon fibers based on C_{60} and their symmetries," *Phys. Rev. B*, Vol. 45, 1992, 6234–6242.
- [53] Schettino, V., Pagliai, M., and Cardini, G., "The Infrared and Raman Spectra of Fullerene C_{70} . DFT Calculations and Correlation with C_{60} ," *J. Chem. Phys. A*, Vol. 106, 2002, 1815–1823.

- [54] van der Pauw, L. J., "A method of measuring the resistivity and Hall coefficient on lamellae of arbitrary shape," *Philips Technical Review*, Vol. 20, 1958/59, 220–224.
- [55] Deng, R., Clegg, A., and Echt, O., "Mass spectrometric study of $K^+ + C_{60}$ collisions," *Int. J. Mass Spectrom.*, Vol. 223, No. 1-3, 2002, 695–710.
- [56] Campbell, E. E. B., Ulmer, G., and Hertel, I. V., "Delayed ionization of C_{60} and C_{70} ," *Phys. Rev. Lett.*, Vol. 67, No. 15, 1991, 1986–1988.
- [57] Rohmund, F., Bulgakov, A. V., Heden, M., Lassesson, A., and Campbell, E. E. B., "Photoionisation and photofragmentation of $Li@C_{60}$," *Chem. Phys. Lett.*, Vol. 323, 2000, 173–179.
- [58] Andreoni, W. and Curioni, A., "Ab initio approach to the structure and dynamics of metallofullerenes," *Appl. Phys. A*, Vol. 66, 1998, 299–306.
- [59] Broć awik, E. and Eilmes, A., "Density functional study of the endohedral complexes $M@C_{60}$ ($M = Li, Na, K, Be, Mg, Ca, La, B, Al$): Electronic properties, ionization potentials, and electron affinities," *J. Chem. Phys.*, Vol. 108, No. 9, 1998, 3498–3503.
- [60] Mitzner, R., Winter, B., Kusch, C., Campbell, E. E. B., and Hertel, I. V., "Coalescence reactions in laser-induced fullerene desorption: the role of fragments," *Z. Phys. D*, Vol. 37, No. 1, 1996, 89–95.
- [61] Yerezian, C., Hansen, K., Diederich, F., and Whetten, R. L., "Coalescence reactions of fullerenes," *Nature*, Vol. 359, 1992, 44–47.
- [62] Beck, R. D., Stoermer, C., Schulz, C., Michel, R., Weis, P., Brauchle, G., and Kappes, M. M., "Enhanced coalescence upon laser desorption of fullerene oxides," *J. Chem. Phys.*, Vol. 101, No. 4, 1994, 3243–3249.
- [63] Ton-That, C., Shard, A. G., Egger, S., Taninaka, A., Shinohara, H., and Welland, M. E., "Structural and electronic properties of ordered $La@C_{82}$ films on Si(111)," *Surf. Sci.*, Vol. 522, No. 1-3, 2003, L15–L20.
- [64] Hebard, A. F., Haddon, R. C., Fleming, R. M., and Kortan, A. R., "Deposition and characterization of fullerene films," *Appl. Phys. Lett.*, Vol. 59, No. 17, 1991, 2109–2111.
- [65] Menéndez, J. and Page, J., " C_{60} vibrations," http://www.public.asu.edu/~cosmen/C60_vibrations/mode_assignments.htm, Accessed 2003-03-24.

- [66] Wågberg, T., Jacobsson, P., and Sundqvist, B., "Comparative Raman study of photopolymerized and pressure-polymerized C₆₀ films," *Phys. Rev. B*, Vol. 60, No. 7, 1999, 4535–4538.
- [67] Kürti, J. and Németh, K., "Structure and energetics of neutral and negatively charged C₆₀ dimers," *Chem. Phys. Lett.*, Vol. 256, 1996, 119–125.
- [68] Scuseria, G. E., "What is the lowest-energy isomer of the C₆₀ dimer?" *Chem. Phys. Lett.*, Vol. 257, 1996, 583–586.
- [69] Oszlányi, G., Bortel, G., Faigel, G., Tegze, M., Gránásy, L., Pekker, S., Stephens, P. W., Bendele, G., Dinnebier, R., Mihály, G., Jánossy, A., Chauvet, O., and Forró, L., "Dimerization in KC₆₀ and RbC₆₀," *Phys. Rev. B*, Vol. 51, 1995, 12228–12232.
- [70] Oszlányi, G., Bortel, G., Faigel, G., Gránásy, L., Bendele, G., Stephens, P. W., and Forró, L., "Single C-C bond in (C₆₀)₂²⁻," *Phys. Rev. B*, Vol. 54, 1996, 11849–11852.
- [71] Plank, W., Pichler, T., Kuzmany, H., Dubay, O., Tagmatarchis, N., and Prasadides, K., "Resonance Raman excitation and electronic structure of the single bonded dimers (C₆₀⁻)₂ and (C₅₉N)₂," *Eur. Phys. J. B*, Vol. 17, 2000, 33–42.
- [72] Rao, A. M., Eklund, P. C., Hodeau, J.-L., Marques, L., and Nunez-Regueiro, M., "Infrared and Raman studies of pressure-polymerized C₆₀," *Phys. Rev. B*, Vol. 55, 1997, 4766–4773.
- [73] Martin, M. C., Koller, D., Rosenberg, A., Kendziora, C., and Mihaly, L., "Infrared and Raman evidence for dimers and polymers in RbC₆₀," *Phys. Rev. B*, Vol. 51, No. 3210-3213, 1995.
- [74] Porezag, D., Jungnickel, G., Frauenheim, T., Seifert, G., Ayuela, A., and Pederson, M. R., "Theoretical investigations of homo- and heteronuclear bridged fullerene oligomers," *Appl. Phys. A*, Vol. 64, 1997, 321–326.
- [75] Lebedkin, S., Hull, W. E., Soldatov, A., Renker, B., and Kappes, M. M., "Structure and Properties of the Fullerene Dimer C₁₄₀ Produced by Pressure Treatment of C₇₀," *J. Chem. Phys. B*, Vol. 104, 2000, 4101–4110.
- [76] Hernández-Rojas, J., Bretón, J., and Gomez Llorente, J. M., "Raman rotational spectra of endohedral C₆₀ fullerene complexes," *J. Chem. Phys.*, Vol. 105, No. 11, 1996, 4482–4487.

- [77] Byszewski, P., Stankowski, J., Trybuła, Z., Kempański, W., and Żuk, T., "EPR and microwave absorption of alkali metal-doped fullerene superconductors," *J. Mol. Struct.*, Vol. 269, No. 1-2, 1992, 175–182.
- [78] Kukolich, S. G. and Huffman, D. R., "EPR spectra of C₆₀ anion and cation radicals," *Chem. Phys. Lett.*, Vol. 182, No. 3-4, 1991, 263–265.
- [79] Popok, V. N., Private communication, 2004.
- [80] Taylor, R., Parsons, J. P., Avent, A. G., Rannard, S. P., Dennis, T. J., Hare, J. P., Kroto, H. W., and Walton, D. R. M., "Degradation of C₆₀ by light," *Nature*, Vol. 351, 1991, 277.
- [81] Milliken, J., Keller, T. M., Baronavski, A. P., McElvany, S. W., Callahan, J. H., and Nelson, H. H., "Thermal and Oxidative Analyses of Buckminsterfullerene, C₆₀," *Chem. Mater.*, Vol. 3, 1991, 386–387.
- [82] Callahan, J. H., McElvany, S. W., and Ross, M. M., "Tandem mass spectrometry studies of oxygen interactions with fullerenes and metallofullerenes," *Int. J. Mass Spectrom. Ion Proc.*, Vol. 138, 1994, 221–239.
- [83] Hettich, R., Lahamer, A., Zhou, L., and Compton, R., "Investigation of the fragmentation and oxygen reactivity of endohedral metallofullerenes M@C₆₀," *Int. J. Mass Spectrom.*, Vol. 182-183, 1999, 335–348.
- [84] Taliani, C., Ruani, G., Zamboni, R., Danieli, R., Rossini, S., Denisov, V. N., Burlakov, V. M., Negri, F., Orlandi, G., and Zerbetto, F., "Light-induced oxygen incision of C₆₀," *J. Chem. Soc. Chem. Commun.*, 1993, 220–222.
- [85] Kroll, G. H., Benning, P. J., Chen, Y., Ohno, T. R., Weaver, J. H., Chibante, L. P. F., and Smalley, R. E., "Interaction of O₂ with C₆₀: photon-induced oxidation," *Chem. Phys. Lett.*, Vol. 181, No. 112-116, 1991.
- [86] Lu, W., Huang, R., and Yang, S., "Efficient formation of molecular oxygen cluster anions in an excimer laser-ablated (308 nm) fullerene source," *Chem. Phys. Lett.*, Vol. 241, No. 4, 1995, 373–379.
- [87] Pevzner, B., Hebard, A. F., and Dresselhaus, M. S., "Role of molecular oxygen and other impurities in the electrical transport and dielectric properties of C₆₀ films," *Phys. Rev. B*, Vol. 55, No. 24, 1997, 16439–16449.
- [88] Ruoff, R. S., Kadish, K. M., Bolas, P., and Chen, E. C. M., "The Relationship between the Electron Affinities and Half-Wave Reduction Potentials of Fullerenes, Aromatic Hydrocarbons, and Metal Complexes," *J. Phys. Chem.*, Vol. 99, No. 21, 1995, 8843–8850.

- [89] Hosoya, M., Ichimura, K., Wang, Z. H., Dresselhaus, G., Dresselhaus, M. S., and Eklund, P. C., "Dark conductivity and photoconductivity in solid films of C_{70} , C_{60} , and K_xC_{70} ," *Phys. Rev. B*, Vol. 49, 1994, 4981–4986.
- [90] Hassan Bhuiyan, M. K. and Mieno, T., "Effect of oxygen on electric conductivities of C_{60} and higher fullerene thin films," *Thin Solid Films*, Vol. 441, No. 1,2, 2003, 187–191.
- [91] Wen, C., Li, J., Kitazawa, K., Aida, T., Honma, I., Komiyama, H., and Yamada, K., "Electrical conductivity of a pure C_{60} single crystal," *Appl. Phys. Lett.*, Vol. 61, No. 18, 1992, 2162–2163.
- [92] Hamed, A., Sun, Y. Y., Tao, Y. K., Meng, R. L., and Hor, P. H., "Effects of oxygen and illumination on the in situ conductivity of C_{60} thin films," *Phys. Rev. B*, Vol. 47, 1993, 10873–10880.

Paper I

Paper II

Paper III